

Rab5 and Alsin regulate stress-activated cytoprotective signaling on mitochondria

FoSheng Hsu¹, Stephanie Spann¹, Charles Ferguson², Tony Hyman¹, Robert G. Parton^{2,3} and Marino Zerial¹

¹Max Planck Institute of Molecular Cell Biology and Genetics, Pfotenhauerstraße 108, 01307 Dresden, Germany.

²Institute for Molecular Bioscience, University of Queensland, Brisbane, Queensland 4072, Australia.

³Centre for Microscopy and Microanalysis, University of Queensland, Brisbane, Queensland 4072, Australia.

To whom correspondence should be addressed.

Email: zerial@mpi-cbg.de

Abstract

Mitochondrial stress response is essential for cell survival, and damaged mitochondria are a hallmark of neurodegenerative diseases. It is thus fundamental to understand how mitochondria relay information within the cell. Here, by investigating mitochondrial-endosome contact sites we made the surprising observation that the small GTPase Rab5 translocates from early endosomes to the outer mitochondrial membrane upon oxidative stress. This is accompanied by an increase in Rab5-positive endosomes in contact with mitochondria. Interestingly, activation of Rab5 on mitochondria depend on the Rab5-GEF ALS2/Alsin, which is encoded by a gene mutated in amyotrophic lateral sclerosis (ALS). *Alsin*^{-/-} human induced pluripotent stem cell-derived spinal motor neurons cannot relocate Rab5 to mitochondria and display increased susceptibility to oxidative stress. These findings define a novel pathway whereby Alsin catalyzes assembly of the Rab5 endocytic machinery on mitochondria. Defects in stress-sensing by endosomes could be crucial for mitochondrial quality control during the onset of ALS.

Keywords: inter-organelle signaling, membrane contact sites, endocytosis, trafficking

Introduction

Mitochondria, the energy “powerhouse” of the cell, play an essential role in a number of other cellular processes such as calcium signaling, lipid synthesis and trafficking, metabolite transport, apoptosis, and reactive oxygen species (ROS) production (Mesmin, 2016, Ott, Gogvadze et al., 2007, Rizzuto, De Stefani et al., 2012). Many of these processes necessitate communication with other cellular compartments. For example, membrane contact sites (MCS) between endoplasmic reticulum and mitochondria are important for Ca^{2+} and lipid transfer (de Brito & Scorrano, 2008), mitochondria fission (Friedman, Lackner et al., 2011), and regulation of apoptosis (Prudent, Zunino et al., 2015). Lipid droplets and peroxisomes interact with mitochondria to regulate fatty acid oxidation (Cohen, Klug et al., 2014, Pu, Ha et al., 2011). Selected membranes can be delivered to peroxisomes and lysosomes via mitochondrial-derived vesicles (Sugiura, McLelland et al., 2014). These examples demonstrate an extensive functional interplay between organelles, either directly via MCS and/or indirectly via vesicular intermediates. However, the underlying molecular mechanisms remain poorly understood and, in particular, the functional relationship between mitochondria and the endocytic system is largely unexplored.

The endocytic pathway is responsible for maintaining cellular homeostasis by internalizing, sorting, recycling and/or degrading distinct types of cargo molecules (Huotari & Helenius, 2011). Rab GTPases serve as molecular signatures for the endosomes, regulating their biogenesis and functions (Pfeffer, 2017, Zerial & McBride, 2001, Zhen & Stenmark, 2015). Ligand-receptor complexes at the plasma membrane (PM) are internalized into early endosomes (EE) marked by small GTPase Rab5, followed by either their recycling back to the PM via Rab4 and Rab11-positive recycling endosomes (RE), or conversion into Rab7-positive late endosomes (LE) *en route* to lysosomes for degradation (Rink, Ghigo et al., 2005, Sonnichsen, De Renzis et al., 2000, Ullrich, Reinsch et al., 1996). On these

endosomal compartments, Rab proteins recruit a plethora of effectors for membrane tethering and fusion, cargo sorting and signaling (Sorkin & von Zastrow, 2009, Stenmark, 2009, Zerial & McBride, 2001). For example, EEA1 is a dimeric coiled-coiled RAb5 effector protein that tethers two vesicles to allow efficient fusion between Rab5-harboured membranes (Murray, Jahn et al., 2016). Other Rab5 effectors such as APPL1 are involved in regulating metabolic and inflammatory responses (Schenck, Goto-Silva et al., 2008, Wen, Yang et al., 2010). Rab activation, and thus stabilization after recruitment, on the membrane requires guanine nucleotide exchange factors (GEFs) (Blumer, Rey et al., 2013). In the case of Rab5, GEFs constitute a family of VPS9 domain-containing proteins, including Rabex-5 (Horiuchi, Lippe et al., 1997), RME-6 (Sato, Sato et al., 2005), amyotrophic lateral sclerosis protein 2 (ALS2/Alsin) (Otomo, Hadano et al., 2003), and mammalian Ras and Rab interactor 1, 2, 3 (Rin1-3) (Hu, Bliss et al., 2005). The rationale behind this complexity is that Rab5 must be specifically regulated by the different GEFs in space and time. The rationale behind this complexity is that Rab5 must be specifically regulated by the different GEFs in space and time. In this respect, the function of many Rab5 GEFs remains unclear.

Physical interactions between the endosomal machinery and mitochondria serve important functions in cell homeostasis, repair and apoptosis. For example, transfer of iron (Das, Nag et al., 2016, Sheftel, Zhang et al., 2007) and cholesterol (Charman, Kennedy et al., 2010) from endosomes to mitochondria is enabled by physical interactions between the two organelles. Another classical example of mitochondria-endo-lysosome interactions is autophagy. Autophagy is a clearance mechanism whereby cells identify defective organelles following damage or stress and eliminate them via the formation of an autophagosome and fusion with lysosomes (Mizushima & Levine, 2010). The mechanism of degrading mitochondria has been termed macroautophagy or mitophagy. Intriguingly, expression of pro-apoptotic factors such as canonical BH3-only proteins drive Rab5- and Rab7-

positive endolysosomes into inner mitochondrial compartments, via a pathway that appears to differ from autophagy/mitophagy (Hamacher-Brady, Choe et al., 2014). Interestingly, our previously conducted genome-wide RNAi screen of endocytosis (Collinet, Stoter et al., 2010) revealed that ~8% of the hit genes had mitochondrial-related functions, pointing at hitherto unexplored molecular connections between the endosomal system and mitochondria. This led us to hypothesize that other mitochondrial functions may be regulated by endocytic components.

Here, by exploring interactions between early endosomes and mitochondria, we made an unexpected observation: we found that upon laser- or chemically-induced oxidative stress in mammalian cells, mitochondria outer membrane permeabilization (MOMP) releases mitochondrial factors such as cytochrome c, and concomitantly, triggers the assembly of the Rab5 machinery on the OMM, in a process independent of mitophagy. Remarkably, we found that the Rab5 GEF responsible for Rab5 activation is Alsln/ALS2, which is also recruited to OMM. Our findings suggest that the Rab endocytic machineries intimately interact with mitochondria during oxidative stress as a cytoprotection mechanism with important implications for amyotrophic lateral sclerosis (ALS) and other neurodegenerative diseases.

Results

Inter-organelle contacts between endosomes and mitochondria.

We first explored the potential physical link between the endosomal system and mitochondria at steady state. In order to capture early endocytic events, HeLa cells stably expressing TagRFP-MTS (mitochondria targeting sequence) (Takeuchi, Kim et al., 2013) were incubated with endocytic cargoes such as Alexa-conjugated transferrin (Tfn) or epidermal growth factor (EGF) for 10 min at 37°C. Cells were fixed and imaged via confocal microscopy. All acquired images were subjected to chromatic shift correction, deconvolution, and localization analysis (MotionTracking) based on subtraction of random colocalization (Kalaidzidis, 2015). Both Tfn and EGF were consistently observed in a subset of endosomes that partially overlapped or were in close proximity to mitochondria (Figure 1A and B). Given that endosomes are motile and omnipresent in the cytoplasm, and the resolution limit of conventional light microscopy, it is difficult to determine whether the observed proximity of endosomes to mitochondria reflects real MCS or simply due to random chance (Kalaidzidis, 2015). One way to approach this problem is to explore how dynamic such inter-organelle contacts are during early endocytic events. To assess the interactions, cells were incubated with Tfn-488 for 1 min to label early endosomes and immediately imaged live using a spinning disk confocal microscope. In the 10-min time-lapsed videos (e.g. Video 1), some organelle interactions were visible between Tfn-containing endosomes and mitochondria labelled by TagRFP-MTS. Endosomal vesicles remained in the proximity or in contact with mitochondria for 3-5 min and, interestingly, we could observe interactions that were followed by fission-like events (Video 2). The live-cell imaging results suggest that the proximity of endosomes and mitochondria observed at steady state (Figure 1) may reflect *bona fide* albeit transient interactions, as suggested previously (Das, Nag et al., 2016, Sheftel, Zhang et al., 2007).

125

126 *Acute mitochondrial stress recruits Rab5 and Rab5-positive endosomes to the outer mitochondrial*
127 *membrane.*

128 Given the key role of mitochondria in sensing and responding to oxidative stress, we asked
129 whether acute perturbation of mitochondria affects endosomes-mitochondria interactions. We used
130 HeLa cells stably expressing GFP-Rab5 under its endogenous promoter with a bacterial artificial
131 chromosome (BAC) transgene (BAC GFP-Rab5) (Villasenor, Nonaka et al., 2015). Live-cell imaging
132 of BAC GFP-Rab5 expressing RFP-MTS frequently confirmed the presence of Rab5-positive early
133 endosomes (>200 nm) in close contact with mitochondria (Video 3). In addition to using an ectopically
134 expressed mitochondrial marker, we also tested other mitochondrial-selective dyes in our live-cell
135 imaging experiments. Unexpectedly, we found that upon prolonged illumination, there was not only a
136 change in mitochondrial morphology but also an alteration in GFP-Rab5 dynamics, with varying levels
137 of increased signal around mitochondria depending on the nature of the dyes. Certain rosamines and
138 rhodamine-derived dyes used to assay mitochondrial functions possess photosensitizing properties
139 (Hsieh, Chu et al., 2015). Therefore, we hypothesized that the change in Rab5 dynamics may be a
140 direct consequence of the change in mitochondrial function.

141 To this end, we applied MitoTracker-Red CMXRos to specifically perturb mitochondrial
142 function (Minamikawa, Sriratana et al., 1999). Consistent with previous reports, low dosage with 561
143 nm laser (~5 J/cm²) caused a decrease in mitochondrial and an increase in cytoplasmic signal,
144 indicative of MOMP, accompanied by globular swelling of mitochondria within min (Figure 1C,
145 Video 4). Surprisingly, laser treatment on MitoTracker-Red labeled cells resulted in translocation of
146 GFP-Rab5 to OMM, marked by an increased in co-localization compared to untreated (Figure 1D).
147 Line scan analysis showed that the recruitment of Rab5 to mitochondria occurred within min post laser

treatment (Figure 1–figure supplement 1A). The Rab5 ring-like signal formed within min and sustained for >60 min where fusion between two mitochondria can be seen (Figure 1E, arrowheads). We also frequently observed the presence of endosomes in proximity to the altered mitochondria (Figure 1C, arrowheads). As controls, cells labeled with MitoTracker Green FM, which does not share the photosensitizing properties reported for MitoTracker-Red CMXRos, or transfected with RFP-MTS retained their tubular structures under the same laser treatment (Figure 1–figure supplement 1B,C), consistent with previous findings (Minamikawa et al., 1999). Additionally, we tested the specificity and localization of the GFP signals by Rab5 and outer mitochondrial membrane protein TOM20 antibodies (Figure 1–figure supplement 2). These results suggest that Rab5 translocates to mitochondria upon MOMP.

Rab5 localizes to regions of mitochondria that are damaged.

We next asked whether GFP-Rab5 relocalization to mitochondria is a general response to overall cell stress or can be elicited locally on individual mitochondria. To test this, we applied stress in a small area within a cell labeled with MitoTracker-Red (Figure 2A, Pre, inset) and monitored the GFP-Rab5 signal after 10 and 20 min (Figure 2B, Post-laser). At 10-minute time after laser irradiation, the MitoTracker-Red signal began to fade. Despite the localized perturbation, we observed an overall change in mitochondrial morphology, from tubular to rounded. This is consistent with the fact that mitochondria form a dynamically interconnected network (Lackner, 2014, Wang, Du et al., 2015) that appears to react to local damage as an ensemble. However, at 20-minute time point, we found strong Rab5 recruitment only in the laser-induced area and not in the rest of the cell (Figure 2B). In the laser-induced area, Rab5 rings formed on rounded mitochondria that exhibited a loss in luminal MitoTracker dye, presumably as a result of MOMP (Figure 2B, arrowheads). We also observed the appearance of

distinct Rab5-positive endosomes contacting these mitochondria (Figure 2B, double arrowheads). These results suggest that Rab5 is recruited in response to signal(s) originated from individually damaged mitochondria.

Membrane contacts between Rab5-positive mitochondria and endosomes.

In our stress-induced conditions, we frequently observed Rab5-positive endosomes in close proximity to the swollen mitochondria (Figure 1C, Figure 2B, double arrowheads, Figure 1–figure supplement 1A). By live-cell imaging, these endosomes also appeared to dock stably onto the mitochondria (Video 5, boxed regions). Due to the diffraction limit of standard light microscopy, we could not resolve objects that are closer than 200 nm and endosomes that are <200 nm in diameter. For these reasons, we complemented our study by correlative light and electron microscopy (CLEM) to obtain ultrastructural details. We designed our experimental setup to 1) image an entire cell live, 2) visualize the translocation of GFP-Rab5 and Rab5-positive endosomes onto mitochondria upon laser-induced stress, and 3) re-image the same cell by serial section transmission electron microscopy (TEM) (Figure 3A). GFP-Rab5 cells labeled with MitoTracker-Red CMXRos were plated on gridded culture dishes, laser-treated and imaged live on the spinning disk confocal microscope. Upon mitochondrial rounding, cells were immediately fixed and re-imaged again to obtain post-fixation image. These showed distinct GFP-positive puncta in close proximity to mitochondria (Figure 3A,B, red arrowhead). Samples were then processed for serial section transmission electron microscopy (TEM) and the same region was re-located in the thin sections by both nuclear membrane (Figure 3B, dotted line) and mitochondria (Figure 3B, red star: mitochondria), acting as fiducial markers. The TEM images from three different serial sections of the inset area in Figure 3B revealed that the GFP-Rab5-positive structure corresponds to a tubular-cisternal structure, approximately 400nm in diameter, with

the typical morphology of an early endosome (Figure 3C, green). Serial section analysis showed that the endosomal membrane was in very close contact (<5 nm) with the adjacent mitochondrion (Figure 3C, red). The rounded mitochondrion showed few cristae, a diameter of approximately $1.5\ \mu\text{m}$, and lacked any additional enveloping membranous structures that might be indicative of mitophagy (Youle & Narendra, 2011). Our data suggest that upon mitochondrial stress, two events involving early endosomes and mitochondria occur: 1) Rab5 translocates to mitochondria and 2) endosomes and mitochondria engage in membrane contacts.

The recruitment of Rab5 to mitochondria is not due to mitophagy.

Following mitochondrial stress, both the timing (in min) of Rab5 recruitment on the rounded mitochondria and the absence of wrapped double-membrane structures argue against mitophagy (Narendra, Tanaka et al., 2008, Novak, Kirkin et al., 2010). We searched for additional evidence to rule out this mechanism. Mitophagy requires the E3 ubiquitin ligase Parkin (Narendra et al., 2008). Parkin is normally located in the cytosol but is recruited to damaged mitochondria, followed by formation of LC3-positive autophagosomes and fusion with Lamp1-positive lysosomes in a process that occurs in hours to days (Dolman, Chambers et al., 2013). To test whether the swollen mitochondria observed in our system undergo this process, we examined the localization of the three markers in BAC GFP-Rab5 cells. We first labeled live cells with MitoTracker-Red CMXRos in order to image mitochondria and endosomes at steady state (Figure 4A,C,E, Untreated) prior to triggering laser-induced stress as before. We then incubated the cells for 60 min as a mean to maximize the time window that these markers might be recruited. Upon fixation, cells were immunostained with specific antibodies to detect endogenous LC3, Lamp1, and Parkin. Since cells were seeded on a gridded dish as positional marker, we were able to re-locate the same cell, which allowed us to assess any changes to

the localization of the different markers as a result of stress when compared to neighboring untreated cells (Figure 4—figure supplement 1). In all laser-induced cells, GFP-Rab5 was specifically enriched around mitochondria when compared to untreated (Figure 4B, D, and F). Sparse LC3 puncta were observed near the perinuclear region in either neighboring untreated or laser-treated cells, where the majority of mitochondria were devoid of any LC3 signals (Figure 4B,G, Figure 4—figure supplement 1A). Similarly, Lamp1 puncta, which mainly resided in the perinuclear region, did not show any change in location in neither untreated nor laser-treated cells (Figure 4D,G, Figure 4—figure supplement 1B). Parkin also remained cytoplasmic and did not show any enrichment around mitochondria upon laser treatment in the time frame of our experiment (Figure 4F,G, Figure 4—figure supplement 1C).

In addition to examining endogenous proteins by immunostaining, we also tested all three markers by live-cell imaging in HeLa BAC cell lines expressing GFP-tagged LC3, Lamp1, and Parkin (Figure 4—figure supplement 2). Cells were laser-induced as before and monitored live for 60 min. As observed with endogenous LC3, a fraction of GFP-LC3 was enriched in the perinuclear region, where it overlapped with small fragmented mitochondria, but not the rest of the mitochondria (Figure 4—figure supplement 2A). We also observed weak GFP-Parkin recruitment to small fragmented mitochondria whereas most mitochondria were devoid of signal in laser-induced conditions (Figure 4—figure supplement 2C, arrowheads). The enrichment to these small fragmented mitochondria may be a result of over-expression which activates some level of mitophagy (Rana, Rera et al., 2013). Nevertheless, unlike Rab5, Parkin was not recruited to the majority of mitochondria. Altogether, the kinetics of Rab5 to stressed mitochondria is indicative of a very fast response (<10 min), the absence of a double membranous structure (Figure 3C) and the lack of significant Parkin recruitment post 3 h

treatment (data not shown) argue that the translocation of Rab5 to mitochondria occurs much earlier than the onset of autophagy and mitophagy.

Rab5 translocation to mitochondria is linked to release of cytochrome c upon hydrogen peroxide treatment.

What could be the signal that drives Rab5 recruitment? Several possible scenarios such as morphological changes to mitochondria and/or release of mitochondrial-derived factor(s) may be accounted for. Morphological changes such as matrix condensation or swelling of mitochondria are often associated with MOMP, cytochrome c release, and subsequent activation of caspases (Gottlieb, Armour et al., 2003). However, this is not a prerequisite. For example, the protonophore carbonyl cyanide m-chlorophenyl hydrazone (CCCP) causes mitochondrial swelling and rounding without immediate cytochrome c release nor cell death (Gao, Pu et al., 2001, Lim, Minamikawa et al., 2001). On the other hand, hydrogen peroxide (H₂O₂) was reported to induce mitochondrial rounding associated with cytochrome c release and caspase activation (Takeyama, Miki et al., 2002). To address this question, we tested CCCP and H₂O₂ on the effect of Rab5 localization. In DMSO control cells, mitochondria were mostly tubular (Figure 5A,B, top panels). The exposure of cells to either CCCP or H₂O₂ for 2 h resulted in mitochondrial rounding, similar to the effect with laser-treatment (Figure 5A,B, bottom panels). Interestingly, Rab5 enrichment on mitochondria was only observed in H₂O₂-treated cells and not in CCCP-treated cells (Figure 5A,B, arrowheads). The enrichment of Rab5 to mitochondria in H₂O₂ condition was ~4-fold higher compared to control cells, as revealed by co-localization analysis (Figure 5C,D).

To corroborate these morphological observations with an independent method, we also tested the effect of H₂O₂ on Rab5 association with endosomes and mitochondria by subcellular fractionation.

We isolated cytosolic and mitochondrial fractions via differential centrifugation and assessed the purity by Western blot analysis using TOM20 as mitochondrial marker and EEA1 as endosomal marker. Consistent with the observation that Rab5 is translocated to stressed mitochondria, we found that cells challenged with H₂O₂ showed a strong increase in the amount of Rab5 present in the mitochondrial fraction (Figure 5E).

We then asked whether the observed difference between CCCP and H₂O₂ could be related to the release of mitochondrial factors such as cytochrome c. To this end, we performed subcellular fractionation on cells treated with either 10 μ M CCCP or 250 μ M H₂O₂ for 2 h. The release of cytochrome c into the cytosol was upregulated in H₂O₂-treated cells, but not in CCCP-treated cells (Figure 5F), consistent with previous reports (Takeyama et al., 2002). Since cytochrome c is a known factor for activating caspase-dependent programmed cell death, we assessed the activity of caspase 3/7 via a 4-amino acid peptide (DEVD) conjugated to a DNA-binding dye. Cleavage of the DEVD peptide by caspase 3/7 releases the DNA-binding fragment, yielding a fluorescent signal. Using flow cytometry, we detected ~62% of cells showing strong fluorescent signal in H₂O₂-treated cells, and merely ~0.6% and ~6.2% in control and CCCP-treated, respectively (Figure 5G).

Altogether, these results show that, in addition to the morphological alterations, the release of cytochrome c and consequent activation of the caspase-dependent apoptotic pathway, H₂O₂ treatment also induces the translocation of Rab5 to mitochondria.

Rab5 translocation to mitochondria blocks caspase release and inhibits trafficking of transferrin upon oxidative stress.

In the course of H₂O₂ treatment by live-cell imaging, we found that mitochondria appeared to respond with different kinetics within an individual cell (Video 6). At the 60-min time point, distinct

regions of the mitochondrial network were more prone to rounding and membrane permeabilization than others, as revealed by the differential loss of MitoTracker-Red signal when compared to control at 0 min (Figure 6A, inset image). Interestingly, these regions correlated exclusively with Rab5 ring-like recruitment (Figure 6A, inset image, arrowheads). This suggests that Rab5 may be involved in either facilitating or preventing the apoptotic process. To address this, we over-expressed either GFP or GFP-Rab5 in HeLa cells and measured the amount of cytosolic cytochrome c at different time points after H₂O₂ addition. We found a significant delay in cytochrome c release from mitochondria in GFP-Rab5 transfected cells compared to control cells (Figure 6B,C). These results suggest that Rab5 plays a protective role in mitochondrial-induced apoptosis by down-regulating the release of pro-apoptotic factors into cytosol.

Given the key role of Rab5 in the biogenesis of the endosomal system (Zeigerer, Gilleron et al., 2012), the dramatic translocation of Rab5 to mitochondria upon oxidative stress by H₂O₂ led us to ask whether endocytic trafficking is affected. To address this, we stimulated HeLa cells with Alexa-647 Tfn continuously for 5 and 10 min. In the absence of H₂O₂, transferrin was present in endosomes throughout the cells and at 10 min accumulated in perinuclear recycling endosomes (Maxfield & McGraw, 2004) (Figure 6D, top). In contrast, cells treated with 250 μ M H₂O₂ showed a severe block in Tfn accumulation at both 5 min and 10 min (Figure 6D,E). This suggests that endosomal trafficking is inhibited during mitochondrial stress, consistent with the reduction of Rab5 on endosomes and its relocation to mitochondria.

Rab5 enrichment on the OMM is accompanied by specific effector recruitment

Since Rab5 translocates from early endosomes to mitochondria, with consequent reduction in endocytic uptake, we next asked whether endosomal Rab5 effectors are also recruited onto

308 mitochondria. We were able to systematically assess the localization of various endosomal effectors
 309 such as Rabenosyn-5/ZFYVE20, EEA1 and APPL1/2 in BAC GFP-Rab5 HeLa cells labeled with
 310 MitoTracker-Red CMXRos via immunostaining by pair-wise combinations. We aimed at detecting the
 311 endogenous rather than the tagged proteins as the latter often cause perturbations and do not
 312 recapitulate the native protein function (Kalaidzidis JCB 2016). The specific antibodies were first
 313 tested in untreated control cells, which all showed significant levels of co-localization with GFP-Rab5
 314 (Figure 7–figure supplement 1). Upon laser-induced stress, the GFP-Rab5 recruitment of Rab5 rings
 315 around mitochondria provided an immediate visual cue and served as positive control. All cells were
 316 fixed after 30 min incubation post-laser treatment. Out of the effectors tested, we detected a strong
 317 enrichment of Rabenosyn-5/ZFYVE20 to mitochondria but not EEA1 in the same cell (Figure 7A,C).
 318 Neither APPL1 nor APPL2 showed enrichment around mitochondria, despite strong Rab5 ring
 319 formation (Figure 7B,C). Unlike Rabenosyn-5/ZFYVE20, EEA1 and APPL1/2 remained well
 320 distributed in endosomal-like vesicles as in both treated and untreated cells (Figure 7B, Figure 7–figure
 321 supplement 1C,D). When we assessed the co-localization of Rab5 and EEA1, there was a loss in co-
 322 localization in laser-treated compared to untreated cells (Figure 7D). The unique localization pattern
 323 led us to ask whether phosphatidylinositol 3-phosphate (PI(3)P) was on OMM in our stress conditions,
 324 since both ZFYVE20/Rabenosyn-5 and EEA1 are recruited to endosomes via both Rab5 and PI(3)P-
 325 binding FYVE motifs (Nielsen, Christofridis et al., 2000). To test this, we over-expressed the PI(3)P
 326 probe GFP-2xFYVE^{Hrs} (Gillooly, Morrow et al., 2000) in HeLa cells and monitored the signals in live
 327 cells upon laser-induced stress. At the initial time point, mitochondria started to retract and swell up,
 328 and the GFP signals were present as vesicle-like puncta (Figure 7–figure supplement 2, 0 min)
 329 consistent with previously reported localization (Gillooly, Morrow et al., 2000). At 60-min elapsed

time point, all mitochondria appeared swollen but were completely devoid of GFP signals, which remained on vesicle-like puncta (Figure 7–figure supplement 2, 60 min).

Our findings reveal a selective mechanism of Rab5 translocation and activation on mitochondria that result in a PI(3)P independent recruitment of specific effectors.

The Rab5 GEF Alsln localizes to mitochondria upon stress induction

Translocation of Rab5 and recruitment of effectors imply that Rab5 must be activated on the mitochondrial membrane. Activation of Rab GTPases on organelle membranes depends on a family of GEFs (Blumer et al., 2013, Pfeffer, 2013, Zerial & McBride, 2001, Zhen & Stenmark, 2015). We first examined the localization of Rabex-5, a known GEF of Rab5 on the endosomal membrane, by immunostaining in BAC GFP-Rab5 cells. Again, we had to localize the endogenous protein because tagged Rabex-5 constructs proved to induce artifacts on the endosomal system (Kalaidzidis and Zerial, unpublished). The formation of GFP-Rab5 rings served as positive control upon laser-treatment. Despite a slight enrichment of endogenous Rabex-5 upon laser-induced stress, the signal appeared mostly as cytosolic and cytoplasmic puncta (Figure 7E), consistent with its endosomal localization (Figure 7–figure supplement 3A).

The weak recruitment of Rabex-5 led us to hypothesize that another GEF might be principally involved. We turned our attention to Alsln as a potential candidate GEF for Rab5 on mitochondria based on several lines of evidence. Alsln is the gene product of ALS2, which is mutated in multiple neurodegenerative disorders such as juvenile amyotrophic lateral sclerosis (ALS), juvenile primary lateral sclerosis (JPLS), and infantile-onset ascending hereditary spastic paralysis (IAHSP). The gene has two splice isoforms, which encodes a long form (LF) of 1657 amino acids and a short form (SF) of 396 amino acids. Alsln-LF comprises of several GEF domains: a RCC1-like domain that acts as GEF

for Ran GTPase, DH-PH domain for Rho GTPase, and a C-terminal VPS9 domain for Rab5 (Topp, Carney et al., 2005) (Figure 7–figure supplement 3B). Functional studies in ALS mouse model have associated Alsin with neuronal survival (Kanekura, Hashimoto et al., 2004, Panzeri, De Palma et al., 2006) and endolysosomal trafficking (Hadano, Mitsui et al., 2016, Hadano, Otomo et al., 2010). Moreover, corticospinal motor neuron (CSMN) in Alsin KO mice display selective defects in mitochondrial morphology (Gautam, Jara et al., 2016). We therefore tested Alsin localization under our stress-induced conditions. At steady state, Alsin was found to localize to vesicular structures, showing only partial overlap with Rab5 (Figure 7–figure supplement 3C). The staining pattern observed is consistent with the reported localization of Alsin (Kanekura et al., 2004, Topp, Gray et al., 2004). In contrast after laser treatment we found strong and uniform Alsin staining around mitochondria (Figure 7F), which showed significant co-localization with mitochondria (Figure 7G). Our data point Alsin as a candidate GEF for activating Rab5 on OMM upon stress induction.

Alsin regulates mitochondrial apoptotic signaling and is required for efficient Rab5 targeting to mitochondria

Several mouse models have been generated for the studies on Alsin. However, these mouse lines failed to recapitulate the phenotypes observed in human patients (Cai, Shim et al., 2008). It has recently been reported that absence of Alsin appear to specifically affect the health of corticospinal motor neurons (Gautam et al., 2016). Therefore, in order to directly probe for the role of Alsin in a more physiological background without compromising our ability for genetic and chemical manipulations, we decided to generate Alsin CRISPR knockout cells in human induced pluripotent stem cells (iPSCs). We confirmed the deletion of Alsin by both PCR and Western blot (Figure 8–figure supplement 1A,B). Importantly, we were able to further differentiate both WT and mutant (Alsin^{-/-})

iPSCs to spinal motor neurons (iPSC-MNs) using a reported protocol (Reinhardt, Glatza et al., 2013). In short, we induced neural progenitor cells (NPC) through embryonic bodies formation by growing iPSC in medium supplemented with transforming growth factor- β (TGF- β) and bone morphogen protein (BMP) small molecule inhibitors (SB431542 and dorsomorphin, respectively), and WNT and Sonic Hedgehog signaling activators (CHIR99021 and PMA, respectively). Differentiation and maturation stages were achieved by culturing cells in retinoic acid (RA), cAMP, and neurotrophic factors (BDNF and GDNF) (Figure 8A). As quality control, high expression of pluripotency markers such as Oct4 and Lin28 were observed in our iPSCs as well as Nestin, Sox2 and Pax6 expression in our neuro-progenitor cells (NPCs) (Figure S8C). Differentiation into mature spinal motor neurons was validated by the expression of choline acetyltransferase (ChAT), HB9, and Islet-1 (ISL1) (Figure 8–figure supplement 1D,E). The cells also showed extensive axonal network as revealed by MAP2 staining. Finally, mature spinal motor neurons were re-tested for expression of Alsin in both WT and Alsin^{-/-} cells (Figure 8–figure supplement 1F).

We first examined the steady state localization of Rab5 and morphology of mitochondria by immunostaining for endogenous Rab5 and TOM20. In iPSC-MNs, Rab5 were present on endosomal-like vesicles ubiquitously in the soma and axon, as expected with its role in retrograde and anterograde transport (Deinhardt, Salinas et al., 2006, Guo, Farias et al., 2016). The mitochondrial network in iPSC-MNs was less tubular and consist of more numerous and smaller rounded mitochondria than those in HeLa cells (Figure 8B, Ctrl). We next wanted to verify whether iPSC-MNs would exhibit the same mitochondrial response to oxidative stress as observed in HeLa cells. Interestingly, we found that iPSC-MNs to be more susceptible to detachment and apoptosis than HeLa cells when challenged with 250 μ M H₂O₂ for 2 h under the same conditions (data not shown). As a result, we optimized the H₂O₂ concentration to 100 μ M for 1 hour such that no immediate cell detachment was observed during the

treatment. Using a lower concentration and shorter incubation time, we then examined the morphology of mitochondria, translocation of endogenous Rab5, association of Rab5 with endosomes and mitochondria, and release of cytochrome c into cytosol. Interestingly, we did not observe significant alterations to mitochondria morphology in both WT and *Alsin*^{-/-} iPSC-MNs. On the other hand, WT iPSC-MNs challenged with H₂O₂ showed robust enrichment of Rab5 on OMM, as observed in HeLa cell, but not in *Alsin*^{-/-} iPSC-MNs (Figure 8B, right panel).

To further corroborate these results, we also performed subcellular fractionation in iPSC-MNs. In untreated control cells, endogenous Rab5 was present solely in the cytosolic fraction and undetectable in the purified mitochondrial fraction (Figure 8C). However, upon challenge with H₂O₂, Rab5 was found to co-fractionate with the mitochondrial fraction in WT iPSC-MNs but only weakly in *Alsin*^{-/-} iPSC-MNs (Figure 8C). The loss of Rab5 in mutant cells correlated with greater susceptibility to H₂O₂–induced apoptosis, as assessed by the rapid release of cytochrome c to the cytosol within an hour and further accumulation at later time points, in comparison to WT cells (Figure 8D). Collectively, our findings demonstrate that *Alsin* is a key regulator for recruiting Rab5 to mitochondria, which together, confer cytoprotective function against oxidative stress.

Discussion:

We discovered a novel cytoprotective mechanism during oxidative stress that entails the translocation of Rab5 from early endosomes to mitochondria. Interestingly, the activation of Rab5 requires ALS2/Alsin, that has also been implicated in early onset ALS. Our results provide an unexpected mechanistic link between the endosomal system and mitochondria that could be of primary importance for the understanding of the mechanism that cause ALS and other neurodegenerative diseases.

Different nutrient or environmental perturbations can affect mitochondria morphology and their metabolic activities such as oxidative phosphorylation and programmed cell death (Galloway & Yoon, 2013). Mitochondria can elicit responses ranging from hypoxia adaptation, inflammation, or programmed cell death when exposed to varying degrees of oxidative stress (Sena & Chandel, 2012). Our findings suggest that the endocytic system is a primary responder to mitochondria under stress. We found that laser- or exogenous ROS (e.g. H₂O₂)-induced damage causes MOMP, mitochondrial swelling, and release of cytochrome c, leading to caspase activation and apoptosis. In these conditions, mitochondria appear to elicit a “cue” to the endosomal system, which results in the recruitment of Alsln and subsequently Rab5 onto OMM to inhibit cytochrome c release and thus, promote cell survival (Figure 9). In the course of this study, Hammerling et al. (Hammerling, Najor et al., 2017) have reported a mitochondrial clearance mechanism by which Rab5-positive early endosomes sequester mitochondria via the ESCRT machinery when cells are treated with FCCP (carbonyl cyanide-p-trifluoromethoxyphenylhydrazone), a derivative compound of CCCP. Our mechanism appears to be distinct from this and previously reported autophagic mechanisms. First, we did not observe engulfment of mitochondria into Rab5-positive early endosomes but recruitment of Alsln, Rab5 and Rabenosyn-5 on mitochondria as well as early endosome-mitochondria interactions in

response to stress. Second, we did not observe such Rab5 recruitment on mitochondria in CCCP-treated cells. One explanation could be attributed to different cell types and lower concentration of CCCP employed in our experiments. Third, the recruitment of Rab5 to damaged mitochondria occurs very rapidly, i.e. within min, well preceding any autophagic components that we analyzed in this study. We found that autophagy is restricted to only a subset of small mitochondrial fragments that are LC3⁺ whereas the majority are devoid of established autophagic markers such as Parkin, LC3 and Lamp1. We cannot rule out that mitochondrial clearance mechanism may still be activated at a later time (see below). We attempted to track the fate of damaged mitochondria in a localized region after laser treatment, but the continuous photoirradiation required to achieve high spatio-temporal resolution also led to quick decrease in MitoTracker Red signal and unwanted additional stress to the cell over time, which prevented us from determining its precise outcome. The loss of MitoTracker signal is likely a result of MOMP and not due to mitochondrial clearance since the OMM can be visualized by TOM20 staining and the presence of the Rab5 ring.

Our data reveal a novel role of Alsin in the activation of the Rab5 machinery on mitochondria to regulate cell defense and survival. Alsin is a protein containing three putative GEF domains: an N-terminal regulator of chromosome condensation 1 (RCC1)-like domain (termed RLD), a middle Dbl homology/pleckstrin homology (DH/PH) domain and a C-terminal VPS9 domain. Besides studies showing the catalytic activity of Alsin VPS9 domain towards Rab5 and its role in endosomal localization and dynamics (Otomo et al., 2003, Topp et al., 2004), the physiological relevance between Alsin and Rab5 has remained mysterious. At steady state, we observe staining of Alsin on vesicular-like structures, consistent with previous reports (Millecamps, Gentil et al., 2005). In stress-induced conditions, however, Alsin and Rab5 re-localized to mitochondria. This suggests a unique mechanism leading to changes in membrane association from endosomal to mitochondrial. Our undifferentiated

Alsin^{-/-} iPS cells showed a partial loss of Rab5 recruitment (data not shown) compared to mature sMN, suggesting that other GEFs may partially compensate for the loss of Alsin, depending on certain conditions. The presence of (low levels of) Rabex-5 on mitochondria (Figure 7G) suggests that this GEF might contribute to Rab5 activation, but cannot fully compensate for Alsin function. Additionally, a homologous gene encoding the protein named ALS2CL, containing just the carboxyl-terminal half of ALS2, is shown to specifically bind to Rab5 and forms a homodimer with full-length Alsin to membranous compartments (Hadano, Otomo et al., 2004, Suzuki-Utsunomiya, Hadano et al., 2007).

Which molecular mechanism is responsible for the dissociation of Rab5 from early endosomes and its recruitment to mitochondria? Several lines of evidence argue that this is a multi-step process that requires a complex cascade of factors and molecular interactions. On early endosomes, a positive feedback loop is sustained by the Rabex-5/Rabaptin-5 complex to maintain or amplify the levels of Rab5 on the membrane (Del Conte-Zerial, Brusch et al., 2008, Lippe, Miaczynska et al., 2001, Zhang, Zhang et al., 2014). However, the stress response introduces instability to such a system. Activation of p38 MAPK by H₂O₂ has been shown to stimulate formation of the GDI:Rab5 complex, thus extracting Rab5 from the early endosome membrane (Cavalli, Vilbois et al., 2001). It is conceivable that such mechanism may account for the mobilization of Rab5 from the endosomal membrane. In addition, p38 MAPK modulates endosomal function via phosphorylation and membrane association of Rab5 effectors (Mace, Miaczynska et al., 2005). We found a reduction in the levels of Rab5 co-localizing with its endosomal effectors (eg. EEA1) (Figure 7D). This may provide an energy-sparing mechanism that overrides Rab5 endosomal interactions in order to slow down endocytosis by relocating part of the Rab5 machinery to mitochondria. Consistent with this idea, Rabaptin-5 is shown to be selectively cleaved by capase-3 during apoptosis, thus affecting its interactions with Rab5 and reducing overall endocytic capacity (Cosulich, Horiuchi et al., 1997, Swanton, Bishop et al., 1999). The loss of

endocytic capacity is supported by the fact that we observed a severe block in transferrin uptake. Such a block may confer another cytoprotective role by reducing iron uptake in order to avoid iron overload and toxicity, which is often observed in neurodegeneration (Nunez, Urrutia et al., 2012). Interestingly, hippocampal HT-22 neurons exposed to excess iron trigger mitochondrial fragmentation and result in decreased cell viability (Park, Lee et al., 2015). As for the activation of Rab5 on mitochondria, the N-terminal RLD of Alsln has been shown to exhibit an autoinhibitory effect on its VPS9 domain (Otomo et al., 2003). We posit that mitochondrial-induced stress triggers structural changes in the protein, releasing the autoinhibitory effect of RLD, thereby exposing the VSP9 domain for Rab5 activation and recruitment.

Besides the decrease in iron uptake to reduce free radical toxicity, a key question is what is the functional significance of the assembly of the Rab5 machinery on mitochondria? It appears that the stress response triggers the remodeling of the OMM to confer molecular features characteristic of the endocytic system. The Rab5 machinery may be used to bring mitochondria in close proximity to early endosomes to form MCS, as these appear to increase upon stress. These MCS may mediate the transfer of lipids and metabolites required for the repair response (Helle, Kanfer et al., 2013). However, the Rab5 translocation may be a priming step of a stress response pathway that could subject the mitochondria to interactions with the entire endo-lysosomal system, eventually leading to autophagy or apoptosis. One quality control mechanism is the formation of mitochondrial-derived vesicles (MDVs), which are involved in the transport of oxidized or damaged cargo to late endosomes and lysosomes for degradation (Soubannier, McLelland et al., 2012). This process primarily depends on PINK1/Parkin (McLelland, Soubannier et al., 2014) but can also occur in a PINK1/Parkin-independent manner (Matheoud, Sugiura et al., 2016). Rab5 could play a role in MDV formation although we could not detect vesicle budding events within our time frame and experimental conditions. Once recruited onto

mitochondria, Rab5 activity may not be limited to the recruitment of its effectors but initiate a more extensive endosomal Rab cascade via the Rab coupling/conversion mechanism. On early endosomes, Rab5 interacts with divalent effectors coupling its activity to Rab proteins (e.g. Rab4, Rab11) required for receptor recycling (de Renzis, Sonnichsen et al., 2002, Vitale, Rybin et al., 1998). Rab5 also initiates activation of Rab7 resulting in conversion of early endosomes into late endosomes (Rink et al., 2005), and consistent with this, silencing of Rab5 in mouse liver causes the loss of the entire endolysosomal system (Zeigerer et al., 2012). Rab coupling/conversion may thus be initiated also on the mitochondria and therefore, it is possible that the mitochondria-endosome MCS may evolve with time leading to the engulfment of mitochondria by the early endosomes (Hammerling, Najor et al., 2017) or to the conventional autophagic processes (Ao, Zou et al., 2014, Stolz, Ernst et al., 2014). It will therefore be important to explore the dynamics of other endosomal Rab GTPases in relation to Rab5 over time.

The physiological role of Alsin has been linked to both endosomes and mitochondria. Cultured hippocampal neurons from Alsin knockout mice display an accumulation of enlarged Rab5 endosomes and reduced endosomal motility (Lai, Xie et al., 2009). Mutational and linkage analysis of Alsin from human patients show that VPS9 domain is critical for Alsin function (Daud, Kakar et al., 2016, Verschuuren-Bemelmans, Winter et al., 2008). Recent EM study on corticospinal motor neurons (CSMN) from Alsin KO mice reveals a selective defect in mitochondria morphology displaying defective membrane and vacuolated cristae (Gautam et al., 2016). Interestingly, WT vs Alsin KO CSMN shows no change in Parkin expression, suggesting that mitophagy does not play a major role. We postulate that the pathological condition of mitochondrial defects in Alsin KO cells is related to a deficiency in Rab5 recruitment to mitochondria, thereby leading to low-levels of protection from ROS

529 accompanying aging. In ALS patients, motor neurons accumulate likely more damaged mitochondria
530 as they age, which eventually become an overload for cells.

531 The cause for ALS is still not fully understood, but oxidative stress is considered to be a major
532 contributor. Mutations in the anti-oxidant enzyme, superoxide dismutase 1 (SOD1), are associated
533 with motor neuron degeneration. Mouse model shows that an accumulation of the SOD1 mutant
534 proteins results in mitochondrial swelling and increased oxidative damage (Jaarsma, Rognoni et al.,
535 2001). Interestingly, loss of Alsin in the mutant SOD1 transgenic mice exacerbates and accelerates
536 disease progression (Hadano et al., 2010). These studies, along with our findings, corroborate the
537 protective role of Alsin during oxidative stress. The mechanistic link between Rab5 and Alsin may
538 present a general or related mechanism in other neurodegenerative diseases. In Parkinson disease, the
539 most common mutation found in the multidomain Leucine-rich repeat kinase 2 (LRRK2) protein leads
540 to hyper-activation of the kinase domain, resulting in hyper-phosphorylation of a number of Rab
541 GTPase substrates including Rab5 (Steger, Tonelli et al., 2016). This may present yet another
542 mechanism of regulating Rab5 localization and function on mitochondria. Future work using different
543 neurodegenerative disease models in differentiated human neurons will provide deeper insights into the
544 disease etiology.

545

546 **Materials and Methods:**

547

548 **Cell lines, cell culture, and growth conditions**

549 HeLa cells were cultured in high glucose DMEM (Gibco) with 10% fetal bovine serum, 100 U/ml
 550 penicillin, 100 µg/ml streptomycin, and 2 mM glutamine (all reagents from Sigma-Aldrich) at 37°C
 551 with 5% CO₂. All plasmids were transfected using Effectene transfection reagent (Qiagen) according
 552 to manufacturer's protocol. All bacterial artificial chromosome (BAC) transgene HeLa cell lines
 553 expressing different markers were obtained from the BAC recombineering facility at MPI-CBG
 554 (Dresden, Germany) and generated using the methods previously described (Poser, Sarov et al., 2008).

555

556 **Plasmids and chemical reagents**

557 Construction of the pEGFP-C3-2xFYVE was constructed using mouse Hrs FYVE domain containing a
 558 linker (QGQGS) (Raiborg, Bremnes et al., 2001). Alexa-conjugated transferrin (Invitrogen; T13342)
 559 and EGF (Invitrogen; E13345) were used at 25 µg/ml and 2 µg/ml, respectively. Carbonyl cyanide 3-
 560 chlorophenylhydrazone (CCCP) was purchased from Sigma Aldrich (C2759). Stock solution was made
 561 to the final concentration of 10 mM in DMSO. Hydrogen peroxide (H₂O₂) (Merck Millipore; 7722-84-
 562 1) 100 mM stock solution was prepared in PBS.

563

564 **Live-cell confocal imaging**

565 Cells were plated in a 35-mm petri dish, 14-mm glass bottom microwell for live-cell imaging. Before
 566 imaging, medium was replaced with HEPES-buffered DMEM without phenol red (Gibco). Cells were
 567 then imaged by time-lapse microscopy (Spinning Disc, Andor-Olympus-IX71 inverted stand
 568 microscope and Nikon TiE inverted stand microscope equipped with spinning disc scan head (CSU-

X1; Yokogawa), fast piezo objective z-positioner [Physik Instrumente], and back-illuminated EMCCD camera (iXon EM+ DU-897 BV; Andor). Imaging was done with an Olympus UPlanSApo 100x 1.4 Oil and Nikon Apo 100x 1.49 Oil DIC 0.13–0.20 objectives (illumination by lasers: DPSS-488nm, DPSS-561nm, DPSS-640nm). Individual planes were recorded at ~10 frames per sec with Z-stacks of three planes (step 0.3 μm).

Photosensitization of mitochondria

Cells were incubated with MitoTracker Red CMXRos (ThermoFisher; M7512) at a final concentration of 100 nM for 30 min at 37°C, 5% CO₂ incubator, and followed by 2X PBS wash before irradiating with 561 nm laser on the spinning disc Andor-Olympus-IX71 at low power dosage of ~5 J/cm² for 60 seconds.

Correlative light electron microscopy

Cells were grown on gridded dish (ibidi μ -Dish 35-mm, high Grid-500). Cells in different locations were laser-treated with 561 nm laser for 30 secs. Cells were fixed in 2.5% glutaraldehyde/PBS for 30 min at room temperature. Post-fixation and embedding were performed using 1% osmium tetroxide/1.5% potassium ferrocyanide and Epon Lx112, respectively. Sectioning of 150 nm thick UA sections was performed on a Leica Ultracut UCT (Leica Microsystem, Wetzlar, Germany) with a diamond knife. Samples are post-stained with 2% uranyl acetate and lead citrate. 2D images were acquired on a Tecnai T12 (FEI, Hillsboro, Oregon, USA).

Immunofluorescence and antibodies

591 Cells were seeded on ibidi Grid-500 glass bottom. After laser or H₂O₂ treatment, cells were fixed in
592 4% paraformaldehyde/PBS for 15 min at room temperature. Cells were washed twice with PBS and
593 permeabilized in PBS containing 0.1% saponin, and 1% BSA for 30 min at room temperature. Cells
594 were immunostained with corresponding primary: anti-rabbit Rabenosyn-5/ZFYVE20 (Sigma Aldrich:
595 HPA044878), anti-mouse EEA1 (BD Biosciences: 610457), anti-rabbit TOM20 (Santa Cruz
596 Biotechnology: sc-11415), anti-rabbit APPL1 (Abcam: ab59592), anti-mouse Rab5 (BD Biosciences:
597 610724), anti-mouse cytochrome c (Abcam: ab6311), and anti-rabbit Alsin (Novus Biological: NBP2-
598 14284) antibodies. Alexa fluor-conjugated from ThermoFisher were used as secondary antibodies.
599 Samples were mounted with Mowiol (Sigma-Aldrich) on glass slides and examined using the Zeiss
600 LSM 880 inverted single photon point scanning confocal system with Quasar detector (32 spectral
601 detection channels in the GaAsP detector plus 2PMTs) and transmitted light detector. Acquired images
602 were processed and saved using the Zeiss ZEN software. For immunofluorescence on iPSCs, smNPCs,
603 and sMNs, cells were fixed with 4 % formaldehyde for 10 min, washed three times with wash buffer
604 (0.3 % Triton-X in PBS) for 5-10 min, and blocked with blocking buffer (5 % goat serum, 2 % BSA,
605 and 0.3 % Triton-X in PBS) for 1 hour at room temperature. Cells were incubated with primary
606 antibody in blocking buffer overnight at 4 °C. After washing three times with PBS for 10 min, cells
607 were incubated with secondary antibodies in wash buffer for 2-3 hours at room temperature followed
608 by three washes in PBS for 10 min. Primary antibodies: goat anti-ChAT (1:100) (Millipore,
609 #AB144P), mouse anti-HB9 (1:50) (DSHB, #81.5C10, conc.), rabbit anti-ISL1 (1:100) (Abcam,
610 #ab20670), mouse anti-LIN28 (1:1000) (Cell signaling, #5930S), chicken anti-MAP2 (1:1000) (Novus
611 Biologicals, #NB300-213), mouse anti-Nestin (1:150) (R&D Systems, #MAB1259), rabbit anti-OCT4
612 (1:500) (Abcam, #ab19857), rabbit anti-PAX6 (1:300) (Covance, #PRB-278P), and rabbit anti-SOX2
613 (1:500) (Abcam, #ab97959).

614

615 **Transferrin uptake**

616 Cells were seeded in a 384-well plate and incubated with either complete medium or in the presence of
617 250 μ M H₂O₂ for 2 hours at 37°C. Cells were then pulsed with Alexa-647 Tfn (10 μ g/ml) for 5 min or
618 10 min, followed by 3x PBS wash, fixed with 3.7% PFA for 15 min, and then stained with DAPI
619 (1:1000) and CellMask Blue (1:2000) (ThermoFisher). Image acquisition was performed via the
620 automated confocal imaging system, CV7000S Yokogawa. Images analysis were performed using
621 MotionTracking software.

622

623 **Subcellular fractionation**

624 Cytosolic and mitochondrial fractions were performed using the mitochondria isolation kit, according
625 to manufacturer's protocol with minor modification (ThermoFisher: cat89874). Cells ($\sim 1 \times 10^7$) were
626 resuspended in 400 μ l Mitochondrial Isolation Reagent A. Cells were chemically lysed by adding 5 μ l
627 of Reagent B. After 5 min incubation on ice, 400 μ l of Reagent C was added to each sample and
628 centrifuged at 720 x g for 10 min. Supernatant was transferred to a new eppendorf tube and centrifuged
629 at 3000 x g for 15 min at 4°C. Supernatant was collected and trichloroacetic acid (TCA)/acetone
630 precipitation was performed to obtain the final cytosolic fraction. The remaining pellet was washed by
631 adding 500 μ l of Reagent C and centrifuged at 15,000 x g for 5 min. Final samples were resuspended
632 in SDS loading buffer.

633

634 **Cytochrome c release assay and Western blot**

635 Cells were seeded onto a 12-well plate. For hydrogen peroxide treatment, reagent was added directly
636 into the well to achieve the appropriate concentration. Separation of mitochondrial and cytosolic

fractions was performed using mitochondrial isolation kit from ThermoFisher (cat:89874) with an additional step of trichloroacetic acid precipitation of the cytosolic fraction. The final pellet was dried for 2-3 min in a 95 °C heat block before resuspending it in SDS loading buffer. Cell lysates were separated by SDS-PAGE, transferred onto nitrocellulose membrane and blocked in 5% milk in PBS containing 0.1% Tween. Primary and secondary antibodies were diluted in blocking buffer and incubated for 2 h at room temperature. Detection of bands was performed using electrochemiluminescence reagent and exposure onto x-ray films. The following antibodies were used by Western blot: anti-mouse cytochrome c (Abcam: ab13575), anti-rabbit gamma tubulin (Sigma-Aldrich: T6557), anti-rabbit Alsin (Sigma Aldrich: SAB4200137), anti-mouse EEA1 (BD Biosciences: 610457), and anti-rabbit TOM20 (Santa Cruz Biotechnology: sc-11415).

Generation of CRISPR/Cas9 knockout in human induced pluripotent cells

Human KOLF_C1 iPSC (kindly provided by Bill Skarnes, Sanger Institute) were cultured in feeder-free conditions on Matrigel with TeSR-E8 media (StemCell, Germany). For ALS2/Alsin knockout using CRISPR/Cas9 genome editing, 350,000 cells were detached using Accutase, washed once with PBS and electroporated using the Neon Transfection System (Invitrogen, Germany, 10ul kit, 1000V, 20ms, 3 pulses). Genomic sequence of human Alsin was analysed for CRISPR/Cas9 target sites by Geneious 8.1.6 software (Biomatters), and two pairs of guides flanking a critical exon (exon3) were selected (5'-GCTAAAGTACTGAATTTTGG-3' and 5'-AATAAAATCAGCAGGTGTGG-3'; 5'-GAATTTCTACAAAGTGCAGG-3' and 5'-TAGCCTGGATGATGGCCGTT-3') and were used together to cause a frame shifting exon deletion). The in vitro efficiency of these gRNAs was assessed by generating genomic PCR cleavage template of 3.4 bp (primers used: for-CCTCCCTTCCCAGGATCTGA and rev-TGCTCAACTCGAGTGCCTTT; for-CAGGGTGAGCATCCCACATT and rev-AGGAGTTCCAGTCAACCACT) and incubating with recombinant Cas9. All gRNAs used in vitro were

identical in sequence to the DNA sense strand and not complementary to the mRNA sequence. The RNAs employed in this method were chemically-modified and length optimized variants of the native guide RNAs (Alt-R™ CRISPR crRNAs and tracrRNA, Integrated DNA Technologies, Coralville, IA, USA). Recombinant Cas9 (provided by Protein Expression Facility at MPI-CBG) protein from *Streptococcus pyogenes* was used. The crRNAs were mixed with tracrRNA and NLS-Cas9 (1 µg/µl). The guide RNA complex was formed by mixing the crRNAs and tracrRNAs in equal amounts in Buffer R (Invitrogen, Germany) at 100µM concentration. 5 days after electroporation, cells were pooled and seeded for clonal dilution. Single clones were mechanically picked and amplified. Next, genomic DNA had been isolated using QuickExtract DNA Extraction Solution (EpiCentre, USA). Homozygous deletions had been verified by PCR and sequencing.

Generation of iPSC-derived smNPC, and differentiation of smNPCs to MNs

All procedures were performed as previously described (Reinhardt et al., 2013). Briefly, for smNPC generation, iPSC colonies detached from Matrigel-coated wells by 1 mg/ml dispase were resuspended in hESC medium (DMEM/F12, 20 % KnockOUT Serum Replacement, 1 % Penicillin/Streptomycin/Glutamine, 0.1 mM Non-Essential Amino Acids Solution, 0.05 mM beta-mercaptoethanol, without bFGF) supplemented with 10 µM SB431542 (Tocris, #1614), 1 µM dorsomorphin (Tocris, #3093), 3 µM CHIR99021 (Axon Medchem, #Axon-1386) and 0.5 µM purmorphamine (STEMCELL Technologies, #72202), and cultured in non-coated petri dishes. After two days, hESC medium was replaced by N2B27 medium (1:1 mixture of DMEM/F12 and Neurobasal medium, 1 % Penicillin/Streptomycin/Glutamine, 1:100 B-27 supplement minus vitamin A, 1:200 N-2 supplement) supplemented with the same small molecules as listed above. After another two days, culture medium was replaced by smNPC expansion medium (N2B27 medium supplemented with 150 µM ascorbic acid (Sigma, #A4403), 3 µM CHIR99021 and 0.5 µM purmorphamine). At day 6 of neural induction, embryonic bodies were broken into smaller clumps by titration and plated in 6 wells of a Matrigel-coated 12-well plate. At day 9, cells were passaged for the first time using Accutase at a 1:3 split ratio and seeded in 4 wells of a Matrigel-coated 6-well plate. Afterwards, cells were passaged ones a week and seeded at a density of 1 x 10⁶

cells per well. To obtain a highly pure smNPC culture, smNPCs were propagated for at least 10 passages in smNPC expansion medium. For differentiation of smNPC to MNs, smNPCs were seeded at a density of 1.5×10^6 cells per one well of a Matrigel-coated 6-well plate and cultured in N2B27 medium supplemented with 1 μ M purmorphamine for the first two days of differentiation. The cells were then cultured in N2B27 medium supplemented with 1 μ M purmorphamine and 1 μ M retinoic acid (Sigma, #R2625) until day 9 of differentiation. At day 9, cells were dissociated using Accutase and plated on polyornithine/laminin-coated ibidi μ -slides (at a density of 150000 cells per well) or Nunc 4-well plates (at a density of 300.000 cells per well) in maturation medium (N2B27 medium supplemented with 0.5 mM cAMP (Sigma, #D0627), 10 ng/ml BDNF (Peprotech, #450-02-10), and 10 ng/ml GDNF (Peprotech, #450-10-10)). Cells were maintained in maturation medium until analysis on day 28.

Image and statistical analysis

Image resizing, cropping and brightness were uniformly adjusted in Fiji (<http://fiji.sc/>). Co-localization analysis was performed using MotionTracking software (Rink et al., 2005) (<http://motiontracking.mpi-cbg.de/get/>) and described previously (Gilleron, Querbes et al., 2013). The y-axis is expressed as the ratio of co-localized objects (eg. A to B) to total objects found in A. Final images were assembled using Adobe Photoshop and Illustrator. Densitometry quantification were performed in Fiji following the previously described protocol (<http://www.yorku.ca/yisheng/Internal/Protocols/ImageJ.pdf>).

Acknowledgements

We thank the MPI-CBG light microscopy facility for access and technical assistance; the TransgeneOmics facility and Hyman lab, especially Mihail Sarov, Aleksandra Syta, Christina Eugster, Kathleen Rönsch, Marit Leuschner, and Ina Poser, for the design, generation, and maintenance of the

709 CRISPR/Cas9 KO iPSC lines; Julia Japtok from the lab of Andreas Hermann for sharing protocols for
 710 the smNPC generation and MN differentiation; Weihua Leng for technical assistance and method
 711 discussion for electron microscopy; Ina Nuesslein and Christina Eugster from the MPI-CBG FACS
 712 facility for assistance on the flow cytometry; Rico Barsacchi from the Technology Development
 713 Studio facility for assistance with the transferrin uptake and access to the Yokogawa system; Yannis
 714 Kalaidzidis for assistance with the MotionTracking software; and Heidi McBride for discussion and
 715 feedbacks.

716

717 **Competing interests**

718 No competing interests exist.

719

References:

- Ao X, Zou L, Wu Y (2014) Regulation of autophagy by the Rab GTPase network. *Cell death and differentiation* 21: 348-58
- Blumer J, Rey J, Dehmelt L, Mazel T, Wu YW, Bastiaens P, Goody RS, Itzen A (2013) RabGEFs are a major determinant for specific Rab membrane targeting. *The Journal of cell biology* 200: 287-300
- Cai H, Shim H, Lai C, Xie C, Lin X, Yang WJ, Chandran J (2008) ALS2/alsin knockout mice and motor neuron diseases. *Neuro-degenerative diseases* 5: 359-66
- Cavalli V, Vilbois F, Corti M, Marcote MJ, Tamura K, Karin M, Arkinstall S, Gruenberg J (2001) The stress-induced MAP kinase p38 regulates endocytic trafficking via the GDI:Rab5 complex. *Mol Cell* 7: 421-32
- Charman M, Kennedy BE, Osborne N, Karten B (2010) MLN64 mediates egress of cholesterol from endosomes to mitochondria in the absence of functional Niemann-Pick Type C1 protein. *Journal of lipid research* 51: 1023-34
- Cohen Y, Klug YA, Dimitrov L, Erez Z, Chuartzman SG, Elinger D, Yofe I, Soliman K, Gartner J, Thoms S, Schekman R, Elbaz-Alon Y, Zalckvar E, Schuldiner M (2014) Peroxisomes are juxtaposed to strategic sites on mitochondria. *Mol Biosyst* 10: 1742-8
- Collinet C, Stoter M, Bradshaw CR, Samusik N, Rink JC, Kenski D, Habermann B, Buchholz F, Henschel R, Mueller MS, Nagel WE, Fava E, Kalaidzidis Y, Zerial M (2010) Systems survey of endocytosis by multiparametric image analysis. *Nature* 464: 243-9
- Cosulich SC, Horiuchi H, Zerial M, Clarke PR, Woodman PG (1997) Cleavage of rabaptin-5 blocks endosome fusion during apoptosis. *The EMBO journal* 16: 6182-91
- Das A, Nag S, Mason AB, Barroso MM (2016) Endosome-mitochondria interactions are modulated by iron release from transferrin. *The Journal of cell biology* 214: 831-45
- Daud S, Kakar N, Goebel I, Hashmi AS, Yaqub T, Nurnberg G, Nurnberg P, Morris-Rosendahl DJ, Wasim M, Volk AE, Kubisch C, Ahmad J, Borck G (2016) Identification of two novel ALS2 mutations in infantile-onset ascending hereditary spastic paraplegia. *Amyotrophic lateral sclerosis & frontotemporal degeneration* 17: 260-5
- de Brito OM, Scorrano L (2008) Mitofusin 2 tethers endoplasmic reticulum to mitochondria. *Nature* 456: 605-10
- de Renzis S, Sonnichsen B, Zerial M (2002) Divalent Rab effectors regulate the sub-compartmental organization and sorting of early endosomes. *Nature cell biology* 4: 124-33
- Deinhardt K, Salinas S, Verastegui C, Watson R, Worth D, Hanrahan S, Bucci C, Schiavo G (2006) Rab5 and Rab7 control endocytic sorting along the axonal retrograde transport pathway. *Neuron* 52: 293-305
- Del Conte-Zerial P, Bruschi L, Rink JC, Collinet C, Kalaidzidis Y, Zerial M, Deutsch A (2008) Membrane identity and GTPase cascades regulated by toggle and cut-out switches. *Mol Syst Biol* 4: 206
- Dolman NJ, Chambers KM, Mandavilli B, Batchelor RH, Janes MS (2013) Tools and techniques to measure mitophagy using fluorescence microscopy. *Autophagy* 9: 1653-62
- Friedman JR, Lackner LL, West M, DiBenedetto JR, Nunnari J, Voeltz GK (2011) ER tubules mark sites of mitochondrial division. *Science* 334: 358-62
- Galloway CA, Yoon Y (2013) Mitochondrial morphology in metabolic diseases. *Antioxidants & redox signaling* 19: 415-30

763 Gao W, Pu Y, Luo KQ, Chang DC (2001) Temporal relationship between cytochrome c release and
764 mitochondrial swelling during UV-induced apoptosis in living HeLa cells. *Journal of cell science* 114:
765 2855-62

766 Gautam M, Jara JH, Sekerkova G, Yasvoina MV, Martina M, Ozdinler PH (2016) Absence of alsin
767 function leads to corticospinal motor neuron vulnerability via novel disease mechanisms. *Human*
768 *molecular genetics* 25: 1074-87

769 Gilleron J, Querves W, Zeigerer A, Borodovsky A, Marsico G, Schubert U, Manygoats K, Seifert S,
770 Andree C, Stoter M, Epstein-Barash H, Zhang L, Koteliensky V, Fitzgerald K, Fava E, Bickle M,
771 Kalaidzidis Y, Akinc A, Maier M, Zerial M (2013) Image-based analysis of lipid nanoparticle-
772 mediated siRNA delivery, intracellular trafficking and endosomal escape. *Nature biotechnology* 31:
773 638-46

774 Gillooly DJ, Morrow IC, Lindsay M, Gould R, Bryant NJ, Gaullier JM, Parton RG, Stenmark H (2000)
775 Localization of phosphatidylinositol 3-phosphate in yeast and mammalian cells. *The EMBO journal*
776 19: 4577-88

777 Gottlieb E, Armour SM, Harris MH, Thompson CB (2003) Mitochondrial membrane potential
778 regulates matrix configuration and cytochrome c release during apoptosis. *Cell death and*
779 *differentiation* 10: 709-17

780 Guo X, Farias GG, Mattera R, Bonifacino JS (2016) Rab5 and its effector FHF contribute to neuronal
781 polarity through dynein-dependent retrieval of somatodendritic proteins from the axon. *Proceedings of*
782 *the National Academy of Sciences of the United States of America* 113: E5318-27

783 Hadano S, Mitsui S, Pan L, Otomo A, Kubo M, Sato K, Ono S, Onodera W, Abe K, Chen X, Koike M,
784 Uchiyama Y, Aoki M, Warabi E, Yamamoto M, Ishii T, Yanagawa T, Shang HF, Yoshii F (2016)
785 Functional links between SQSTM1 and ALS2 in the pathogenesis of ALS: cumulative impact on the
786 protection against mutant SOD1-mediated motor dysfunction in mice. *Human molecular genetics* 25:
787 3321-3340

788 Hadano S, Otomo A, Kunita R, Suzuki-Utsunomiya K, Akatsuka A, Koike M, Aoki M, Uchiyama Y,
789 Itoyama Y, Ikeda JE (2010) Loss of ALS2/Alsin exacerbates motor dysfunction in a SOD1-expressing
790 mouse ALS model by disturbing endolysosomal trafficking. *PloS one* 5: e9805

791 Hadano S, Otomo A, Suzuki-Utsunomiya K, Kunita R, Yanagisawa Y, Showguchi-Miyata J,
792 Mizumura H, Ikeda JE (2004) ALS2CL, the novel protein highly homologous to the carboxy-terminal
793 half of ALS2, binds to Rab5 and modulates endosome dynamics. *FEBS letters* 575: 64-70

794 Hamacher-Brady A, Choe SC, Krijnse-Locker J, Brady NR (2014) Intramitochondrial recruitment of
795 endolysosomes mediates Smac degradation and constitutes a novel intrinsic apoptosis antagonizing
796 function of XIAP E3 ligase. *Cell death and differentiation* 21: 1862-76

797 Hammerling BC, Najor RH, Cortez MQ, Shires SE, Leon LJ, Gonzalez ER, Boassa D, Phan S, Thor A,
798 Jimenez RE, Li H, Kitsis RN, Dorn II GW, Sadoshima J, Ellisman MH, Gustafsson AB (2017) A Rab5
799 endosomal pathway mediates Parkin-dependent mitochondrial clearance. *Nat Commun* 8: 14050

800 Helle SC, Kanfer G, Kolar K, Lang A, Michel AH, Kornmann B (2013) Organization and function of
801 membrane contact sites. *Biochimica et biophysica acta* 1833: 2526-41

802 Horiuchi H, Lippe R, McBride HM, Rubino M, Woodman P, Stenmark H, Rybin V, Wilm M, Ashman
803 K, Mann M, Zerial M (1997) A novel Rab5 GDP/GTP exchange factor complexed to Rabaptin-5 links
804 nucleotide exchange to effector recruitment and function. *Cell* 90: 1149-59

805 Hsieh CW, Chu CH, Lee HM, Yuan Yang W (2015) Triggering mitophagy with far-red fluorescent
806 photosensitizers. *Scientific reports* 5: 10376

807 Hu HL, Bliss JM, Wang Y, Colicelli J (2005) RIN1 is an ABL tyrosine kinase activator and a regulator
808 of epithelial-cell adhesion and migration. *Current Biology* 15: 815-823

Huotari J, Helenius A (2011) Endosome maturation. *The EMBO journal* 30: 3481-500

Jaarsma D, Rognoni F, van Duijn W, Verspaget HW, Haasdijk ED, Holstege JC (2001) CuZn superoxide dismutase (SOD1) accumulates in vacuolated mitochondria in transgenic mice expressing amyotrophic lateral sclerosis-linked SOD1 mutations. *Acta neuropathologica* 102: 293-305

Kalaidzidis YK, I.; Zerial, M. (2015) A probabilistic method to quantify the colocalization of markers on intracellular vesicular structures visualized by light microscopy. *Aip Conf Proc* 1641: 580-587

Kanekura K, Hashimoto Y, Niikura T, Aiso S, Matsuoka M, Nishimoto I (2004) Alsin, the product of ALS2 gene, suppresses SOD1 mutant neurotoxicity through RhoGEF domain by interacting with SOD1 mutants. *The Journal of biological chemistry* 279: 19247-56

Lackner LL (2014) Shaping the dynamic mitochondrial network. *BMC Biol* 12: 35

Lai C, Xie C, Shim H, Chandran J, Howell BW, Cai H (2009) Regulation of endosomal motility and degradation by amyotrophic lateral sclerosis 2/alsin. *Molecular brain* 2: 23

Lim ML, Minamikawa T, Nagley P (2001) The protonophore CCCP induces mitochondrial permeability transition without cytochrome c release in human osteosarcoma cells. *FEBS letters* 503: 69-74

Lippe R, Miaczynska M, Rybin V, Runge A, Zerial M (2001) Functional synergy between Rab5 effector Rabaptin-5 and exchange factor Rabex-5 when physically associated in a complex. *Molecular biology of the cell* 12: 2219-28

Mace G, Miaczynska M, Zerial M, Nebreda AR (2005) Phosphorylation of EEA1 by p38 MAP kinase regulates mu opioid receptor endocytosis. *The EMBO journal* 24: 3235-46

Matheoud D, Sugiura A, Bellemare-Pelletier A, Laplante A, Rondeau C, Chemali M, Fazel A, Bergeron JJ, Trudeau LE, Burelle Y, Gagnon E, McBride HM, Desjardins M (2016) Parkinson's Disease-Related Proteins PINK1 and Parkin Repress Mitochondrial Antigen Presentation. *Cell* 166: 314-327

Maxfield FR, McGraw TE (2004) Endocytic recycling. *Nature reviews Molecular cell biology* 5: 121-32

McLelland GL, Soubannier V, Chen CX, McBride HM, Fon EA (2014) Parkin and PINK1 function in a vesicular trafficking pathway regulating mitochondrial quality control. *The EMBO journal* 33: 282-95

Mesmin B (2016) Mitochondrial lipid transport and biosynthesis: A complex balance. *The Journal of cell biology* 214: 9-11

Millecamps S, Gentil BJ, Gros-Louis F, Rouleau G, Julien JP (2005) Alsin is partially associated with centrosome in human cells. *Biochimica et biophysica acta* 1745: 84-100

Minamikawa T, Sriratana A, Williams DA, Bowser DN, Hill JS, Nagley P (1999) Chloromethyl-X-rosamine (MitoTracker Red) photosensitises mitochondria and induces apoptosis in intact human cells. *Journal of cell science* 112 (Pt 14): 2419-30

Mizushima N, Levine B (2010) Autophagy in mammalian development and differentiation. *Nature cell biology* 12: 823-30

Murray DH, Jahnel M, Lauer J, Avellaneda MJ, Brouilly N, Cezanne A, Morales-Navarrete H, Perini ED, Ferguson C, Lupas AN, Kalaidzidis Y, Parton RG, Grill SW, Zerial M (2016) An endosomal tether undergoes an entropic collapse to bring vesicles together. *Nature* 537: 107-111

Narendra D, Tanaka A, Suen DF, Youle RJ (2008) Parkin is recruited selectively to impaired mitochondria and promotes their autophagy. *The Journal of cell biology* 183: 795-803

Nielsen E, Christoforidis S, Uttenweiler-Joseph S, Miaczynska M, Dewitte F, Wilm M, Hoflack B, Zerial M (2000) Rabenosyn-5, a novel Rab5 effector, is complexed with hVPS45 and recruited to endosomes through a FYVE finger domain. *The Journal of cell biology* 151: 601-12

855 Nielsen E, Severin F, Backer JM, Hyman AA, Zerial M (1999) Rab5 regulates motility of early
856 endosomes on microtubules. *Nature cell biology* 1: 376-82

857 Novak I, Kirkin V, McEwan DG, Zhang J, Wild P, Rozenknop A, Rogov V, Lohr F, Popovic D,
858 Occhipinti A, Reichert AS, Terzic J, Dotsch V, Ney PA, Dikic I (2010) Nix is a selective autophagy
859 receptor for mitochondrial clearance. *EMBO Rep* 11: 45-51

860 Nunez MT, Urrutia P, Mena N, Aguirre P, Tapia V, Salazar J (2012) Iron toxicity in
861 neurodegeneration. *Biometals* 25: 761-76

862 Otomo A, Hadano S, Okada T, Mizumura H, Kunita R, Nishijima H, Showguchi-Miyata J,
863 Yanagisawa Y, Kohiki E, Suga E, Yasuda M, Osuga H, Nishimoto T, Narumiya S, Ikeda JE (2003)
864 ALS2, a novel guanine nucleotide exchange factor for the small GTPase Rab5, is implicated in
865 endosomal dynamics. *Human molecular genetics* 12: 1671-87

866 Ott M, Gogvadze V, Orrenius S, Zhivotovsky B (2007) Mitochondria, oxidative stress and cell death.
867 *Apoptosis* 12: 913-22

868 Panzeri C, De Palma C, Martinuzzi A, Daga A, De Polo G, Bresolin N, Miller CC, Tudor EL,
869 Clementi E, Bassi MT (2006) The first ALS2 missense mutation associated with JPLS reveals new
870 aspects of alsin biological function. *Brain* 129: 1710-9

871 Park J, Lee DG, Kim B, Park SJ, Kim JH, Lee SR, Chang KT, Lee HS, Lee DS (2015) Iron overload
872 triggers mitochondrial fragmentation via calcineurin-sensitive signals in HT-22 hippocampal neuron
873 cells. *Toxicology* 337: 39-46

874 Pfeffer SR (2013) Rab GTPase regulation of membrane identity. *Curr Opin Cell Biol* 25: 414-9

875 Pfeffer SR (2017) Rab GTPases: master regulators that establish the secretory and endocytic pathways.
876 *Molecular biology of the cell* 28: 712-715

877 Poser I, Sarov M, Hutchins JR, Heriche JK, Toyoda Y, Pozniakovsky A, Weigl D, Nitzsche A,
878 Hegemann B, Bird AW, Pelletier L, Kittler R, Hua S, Naumann R, Augsburg M, Sykora MM,
879 Hofemeister H, Zhang Y, Nasmyth K, White KP et al. (2008) BAC TransgeneOmics: a high-
880 throughput method for exploration of protein function in mammals. *Nature methods* 5: 409-15

881 Prudent J, Zunino R, Sugiura A, Mattie S, Shore GC, McBride HM (2015) MAPL SUMOylation of
882 Drp1 Stabilizes an ER/Mitochondrial Platform Required for Cell Death. *Mol Cell* 59: 941-55

883 Pu J, Ha CW, Zhang S, Jung JP, Huh WK, Liu P (2011) Interactomic study on interaction between
884 lipid droplets and mitochondria. *Protein Cell* 2: 487-96

885 Raiborg C, Bremnes B, Mehlum A, Gillooly DJ, D'Arrigo A, Stang E, Stenmark H (2001) FYVE and
886 coiled-coil domains determine the specific localisation of Hrs to early endosomes. *Journal of cell*
887 *science* 114: 2255-63

888 Rana A, Rera M, Walker DW (2013) Parkin overexpression during aging reduces proteotoxicity, alters
889 mitochondrial dynamics, and extends lifespan. *Proceedings of the National Academy of Sciences of*
890 *the United States of America* 110: 8638-43

891 Reinhardt P, Glatza M, Hemmer K, Tsytsyura Y, Thiel CS, Hoing S, Moritz S, Parga JA, Wagner L,
892 Bruder JM, Wu G, Schmid B, Ropke A, Klingauf J, Schwamborn JC, Gasser T, Scholer HR,
893 Sternecker J (2013) Derivation and expansion using only small molecules of human neural
894 progenitors for neurodegenerative disease modeling. *PloS one* 8: e59252

895 Rink J, Ghigo E, Kalaidzidis Y, Zerial M (2005) Rab conversion as a mechanism of progression from
896 early to late endosomes. *Cell* 122: 735-49

897 Rizzuto R, De Stefani D, Raffaello A, Mammucari C (2012) Mitochondria as sensors and regulators of
898 calcium signalling. *Nature reviews Molecular cell biology* 13: 566-78

899 Sato M, Sato K, Fonarev P, Huang CJ, Liou W, Grant BD (2005) *Caenorhabditis elegans* RME-6 is a
900 novel regulator of RAB-5 at the clathrin-coated pit. *Nature cell biology* 7: 559-69

901 Schenck A, Goto-Silva L, Collinet C, Rhinn M, Giner A, Habermann B, Brand M, Zerial M (2008)
 902 The endosomal protein Appl1 mediates Akt substrate specificity and cell survival in vertebrate
 903 development. *Cell* 133: 486-97
 904 Sena LA, Chandel NS (2012) Physiological roles of mitochondrial reactive oxygen species. *Mol Cell*
 905 48: 158-67
 906 Sheftel AD, Zhang AS, Brown C, Shirihai OS, Ponka P (2007) Direct interorganellar transfer of iron
 907 from endosome to mitochondrion. *Blood* 110: 125-32
 908 Sonnichsen B, De Renzis S, Nielsen E, Rietdorf J, Zerial M (2000) Distinct membrane domains on
 909 endosomes in the recycling pathway visualized by multicolor imaging of Rab4, Rab5, and Rab11. *The*
 910 *Journal of cell biology* 149: 901-14
 911 Sorkin A, von Zastrow M (2009) Endocytosis and signalling: intertwining molecular networks. *Nature*
 912 *reviews Molecular cell biology* 10: 609-22
 913 Soubannier V, McLelland GL, Zunino R, Braschi E, Rippstein P, Fon EA, McBride HM (2012) A
 914 vesicular transport pathway shuttles cargo from mitochondria to lysosomes. *Current biology* : CB 22:
 915 135-41
 916 Steger M, Tonelli F, Ito G, Davies P, Trost M, Vetter M, Wachter S, Lorentzen E, Duddy G, Wilson S,
 917 Baptista MAS, Fiske BK, Fell MJ, Morrow JA, Reith AD, Alessi DR, Mann M (2016)
 918 Phosphoproteomics reveals that Parkinson's disease kinase LRRK2 regulates a subset of Rab GTPases.
 919 *eLife* 5
 920 Stenmark H (2009) Rab GTPases as coordinators of vesicle traffic. *Nature reviews Molecular cell*
 921 *biology* 10: 513-25
 922 Stenmark H, Parton RG, Steele-Mortimer O, Lutcke A, Gruenberg J, Zerial M (1994) Inhibition of
 923 rab5 GTPase activity stimulates membrane fusion in endocytosis. *The EMBO journal* 13: 1287-96
 924 Stolz A, Ernst A, Dikic I (2014) Cargo recognition and trafficking in selective autophagy. *Nature cell*
 925 *biology* 16: 495-501
 926 Sugiura A, McLelland GL, Fon EA, McBride HM (2014) A new pathway for mitochondrial quality
 927 control: mitochondrial-derived vesicles. *The EMBO journal* 33: 2142-56
 928 Suzuki-Utsunomiya K, Hadano S, Otomo A, Kunita R, Mizumura H, Osuga H, Ikeda JE (2007)
 929 ALS2CL, a novel ALS2-interactor, modulates ALS2-mediated endosome dynamics. *Biochem Biophys*
 930 *Res Commun* 354: 491-7
 931 Swanton E, Bishop N, Woodman P (1999) Human rabaptin-5 is selectively cleaved by caspase-3
 932 during apoptosis. *The Journal of biological chemistry* 274: 37583-90
 933 Takeuchi A, Kim B, Matsuoka S (2013) The mitochondrial Na⁺-Ca²⁺ exchanger, NCLX, regulates
 934 automaticity of HL-1 cardiomyocytes. *Scientific reports* 3: 2766
 935 Takeyama N, Miki S, Hirakawa A, Tanaka T (2002) Role of the mitochondrial permeability transition
 936 and cytochrome C release in hydrogen peroxide-induced apoptosis. *Experimental cell research* 274:
 937 16-24
 938 Topp JD, Carney DS, Horazdovsky BF (2005) Biochemical characterization of Alsln, a Rab5 and Rac1
 939 guanine nucleotide exchange factor. *Methods Enzymol* 403: 261-76
 940 Topp JD, Gray NW, Gerard RD, Horazdovsky BF (2004) Alsln is a Rab5 and Rac1 guanine nucleotide
 941 exchange factor. *The Journal of biological chemistry* 279: 24612-23
 942 Ullrich O, Reinsch S, Urbe S, Zerial M, Parton RG (1996) Rab11 regulates recycling through the
 943 pericentriolar recycling endosome. *The Journal of cell biology* 135: 913-24
 944 Verschuuren-Bemelmans CC, Winter P, Sival DA, Elting JW, Brouwer OF, Muller U (2008) Novel
 945 homozygous ALS2 nonsense mutation (p.Gln715X) in sibs with infantile-onset ascending spastic

paralysis: the first cases from northwestern Europe. *European journal of human genetics* : EJHG 16: 1407-11

Villasenor R, Nonaka H, Del Conte-Zerial P, Kalaidzidis Y, Zerial M (2015) Regulation of EGFR signal transduction by analogue-to-digital conversion in endosomes. *eLife* 4

Vitale G, Rybin V, Christoforidis S, Thornqvist P, McCaffrey M, Stenmark H, Zerial M (1998) Distinct Rab-binding domains mediate the interaction of Rabaptin-5 with GTP-bound Rab4 and Rab5. *The EMBO journal* 17: 1941-51

Wang C, Du W, Su QP, Zhu M, Feng P, Li Y, Zhou Y, Mi N, Zhu Y, Jiang D, Zhang S, Zhang Z, Sun Y, Yu L (2015) Dynamic tubulation of mitochondria drives mitochondrial network formation. *Cell Res* 25: 1108-20

Wen L, Yang Y, Wang Y, Xu A, Wu D, Chen Y (2010) *Appl1* is essential for the survival of *Xenopus* pancreas, duodenum, and stomach progenitor cells. *Developmental dynamics* : an official publication of the American Association of Anatomists 239: 2198-207

Youle RJ, Narendra DP (2011) Mechanisms of mitophagy. *Nature reviews Molecular cell biology* 12: 9-14

Zeigerer A, Gilleron J, Bogorad RL, Marsico G, Nonaka H, Seifert S, Epstein-Barash H, Kuchimanchi S, Peng CG, Ruda VM, Del Conte-Zerial P, Hengstler JG, Kalaidzidis Y, Koteliensky V, Zerial M (2012) Rab5 is necessary for the biogenesis of the endolysosomal system in vivo. *Nature* 485: 465-70

Zerial M, McBride H (2001) Rab proteins as membrane organizers. *Nature reviews Molecular cell biology* 2: 107-17

Zhang Z, Zhang T, Wang S, Gong Z, Tang C, Chen J, Ding J (2014) Molecular mechanism for Rabex-5 GEF activation by Rabaptin-5. *eLife* 3

Zhen Y, Stenmark H (2015) Cellular functions of Rab GTPases at a glance. *Journal of cell science* 128: 3171-6

Figure Legends:

Figure 1. Recruitment of Rab5 to the outer mitochondrial membrane (OMM) upon mitochondrial stress. (A) and (B) HeLa cells were transfected with TagRFP-MTS (mitochondria targeting sequence) and labeled with either Alexa-488 transferrin (Tfn) or epidermal growth factor (EGF), respectively. (C) Live BAC GFP-Rab5 HeLa cells were labeled with 100 nM MitoTracker-Red CMXRos for 30 min at 37°C. Cells were photoirradiated with low dosage of 561 nm laser ($\sim 5 \text{ J/cm}^2$) for 60 sec. Snapshot of the cell was taken at 15 min post-laser treatment. Arrowheads indicate GFP-Rab5-positive endosomes that are in close proximity to mitochondria. (D) Quantification of colocalization before (Untreated) and post-laser treatment (Laser-induced), $n = 3$. The y-axis is defined as the ratio of the amount of MitoTracker-Red colocalized with GFP-Rab5 to the total amount of MitoTracker-Red. Error bars represent SEMs. (E) Time-lapse images of a cell following laser treatment. Inset images are shown at different time points (min). Arrowheads indicate recruitment of GFP-Rab5 to the mitochondria within 15 min, which persist over a period of 60 min. Scale bars, 10 μm .

Figure 1–figure supplement 1. Rab5 recruitment to mitochondria occurs within min and is specific to MitoTracker-Red CMXRos. (A) HeLa BAC GFP-Rab5 cells labeled with MitoTracker-Red CMXRos were photoirradiated with low dosage of 561 nm laser ($\sim 5 \text{ J/cm}^2$) for 60 sec. Snapshot of a cell was taken immediately after photoirradiation (0 min) and 2 min elapsed. Inset images show the rapid recruitment of Rab5 signal (green) around mitochondria (red) via line trace (red: Mito-Red; green: GFP-Rab5). Arrowheads indicate endosomes that are in close proximity to mitochondria. (B) HeLa cells were labeled with MitoTracker-Green FM (Mito-Green) and photoirradiated with 561 nm laser ($\sim 10 \text{ J/cm}^2$) for 60 sec. Image was taken 20 min post-laser. Mitochondrial network remained

tubular. (C) HeLa BAC GFP-Rab5 cells were transfected with TagRFP-MTS and photoirradiated with 561 nm laser ($\sim 10 \text{ J/cm}^2$) for 60 sec. Image was taken 20 min post-laser. Scale bars, 10 μm .

Figure 1—figure supplement 2. Localization of GFP-Rab5 signals assessed by Rab5 and TOM20 antibodies. BAC GFP-Rab5 cells were seeded on gridded glass bottom, labeled with MitoTracker-Red CMXRos, photoirradiated as before, and fixed after 30 min post-laser. Cells were then immunostained with specific antibodies against Rab5 or TOM20. Scale bars, 10 μm .

Figure 2. Rab5 is signaled onto localized damaged mitochondria. (A) BAC GFP-Rab5 cells were labeled with 100 nM MitoTracker-Red CMXRos for 30 min at 37°C, and imaged live. A cell before laser treatment is shown (Pre). (B) Photoirradiation was applied as before to a localized region within the cell (white box). Snapshot of the cell was taken at 10 min and 20 min post-laser. Inset images indicate the effect of laser treatment on mitochondrial morphology and network. Arrowheads indicate the recruitment of GFP-Rab5 (filled) and GFP-Rab5-positive endosomes near the OMM (double-line) at 20 min time point. Scale bars, 10 μm .

Figure 3. Membrane contacts between Rab5-positive mitochondria and endosomes.

Ultrastructural analysis of cells upon laser-induced stress. (A) Flow chart of the experimental set up. BAC GFP-Rab5 cells were seeded onto gridded dish, labeled with MitoTracker-Red CMXRos. The motility of GFP-Rab5-positive endosomes were briefly assessed as a readout for healthy and active cells. A cell of interest was then photoirradiated with lower dosage of 561 nm laser. (B) Fluorescence images of GFP-Rab5 and MitoTracker-Red after fixation with glutaraldehyde. Box region shows a GFP-Rab5 endosome (arrowhead) next to a swollen mitochondrion. The transmission electron

micrograph (TEM) of the same cell is shown. The nuclear membrane (dotted line) and mitochondria (red star) were used as fiducial markers to re-locate the same cell. (C) Zoom-in images of the box region in (B). Colored images indicate GFP-Rab5-positive structure in green and mitochondria in red. Raw images are shown below. Mitochondrial cristae are visible.

Figure 4. Localization of endogenous LC3, Lamp1, and Parkin upon mitochondrial stress. BAC GFP-Rab5 cells were labeled with 100 nm of MitoTracker-Red CMXRos for 30 min at 37°C. Snapshot images of cells were taken as control (Untreated) (A), (C), and (E). The same cells were photoirradiated as before, fixed after 60-min elapsed, and labeled with specific antibodies against LC3 (B), Lamp1 (D), and Parkin (F), respectively. Inset images indicate the approximate area before and after laser treatment. (G) Quantification of colocalization of MitoTracker-Red to Rab5, LC3, Lamp1, and Parkin, respectively, in untreated versus laser-induced conditions ($n = 3$). Untreated cells correspond to cells outside of laser treated area. Scale bars, 10 μ m.

Figure 4—figure supplement 1. Localization of endogenous LC3, Lamp1, and Parkin in untreated cells. BAC GFP-Rab5 cells were seeded on gridded glass bottom, and labeled with MitoTracker-Red CMXRos. Fixed cells were immunostained with specific antibodies against LC3, Lamp1, and Parkin. Cells shown were imaged from area outside of laser-treated cells. Scale bars, 10 μ m.

Figure 4—figure supplement 2. BAC GFP-LC3, GFP-Lamp1, and GFP-Parkin localization upon laser-induced stress. Live-cell imaging of different BAC cell lines. Cells were labeled with MitoTracker-Red CMXRos and photoirradiated as before. Images of the same cell in pre- (untreated) and post-laser are shown. Inset images indicate the approximate area before and after laser treatment.

(A) Images of BAC GFP-LC3 cell before and 60 min post-laser. (B) Images of BAC GFP-Lamp1 cell before and 60 min post-laser. (C) Images of BAC GFP-Parkin cell before and 60 min post-laser. Scale bars, 10 μ m.

Figure 5. Effects of carbonyl cyanide m-chlorophenyl hydrazone (CCCP) and hydrogen peroxide

(H₂O₂) on Rab5 recruitment to mitochondria. (A) Cells were treated with either DMSO (Ctrl) or 10 μ M CCCP for 2 h. (B) Cell were treated with either DMSO (Ctrl) or 250 μ M H₂O₂ for 2 h. Cells were fixed and imaged by confocal microscopy. Inset regions show the effect of the treatment on mitochondrial morphology, and GFP-Rab5 localization. Arrowheads point to rounded mitochondria in both CCCP- and H₂O₂- treated conditions. (C) and (D) Quantification of colocalization in (A) and (B), respectively. $n = 10$. resulted in robust recruitment of GFP-Rab5. (E) Subcellular fractionation of cytosolic (Cyto) and mitochondrial (Mito) fractions from HeLa cells treated with either PBS (control) or 250 μ M H₂O₂ for 2 h at 37°C. Protein samples were loaded onto SDS-PAGE and immunoblotted with Rab5, EEA1, and TOM20 antibodies. (F) Subcellular fractionation of HeLa cells treated with DMSO, 10 μ M CCCP, or 250 μ M H₂O₂ for 2 h. Protein samples from purified mitochondria (Mito) and cytosolic (Cyto) fractions were loaded onto SDS-PAGE and imunoblotted with cytochrome c antibody by Western blot. (G) Cells were treated the same way as in (F). Cells were then resuspended in live-cell imaging solution containing 500 nM caspase-3/7 green flow cytometric reagent and incubated for 30 min at 37°C before subjecting to flow cytometric analysis. FITC signal (x-axis) is plotted against total cell count (y-axis). Gating was set based on background signal in DMSO control. Error bars represent SEMs.

Figure 6. Rab5 regulates mitochondrial-induced apoptosis by blocking cytochrome c release. (A)

Representative images of a live BAC GFP-Rab5 cell before (0 min) and after treatment with 250 μ M H₂O₂ for 60 min. MitoTracker-Red CMXRos was used to monitor MOMP events as shown in the inset images (right panel, arrowheads). Scale bars, 10 μ m. **(B)** HeLa cells over-expressing either GFP or GFP-Rab5 were treated with 250 μ M H₂O₂ at different time points (1 hr to 4 hr). Protein samples from purified cytosolic fraction were obtained and immunoblotted with cytochrome c antibody by Western blot. Tubulin was included as loading control. **(C)** Densitometric quantification from the Western blots performed in **(B)**. Data were collected from three independent experiments ($n = 3$). Y-axis corresponds to normalized ratio intensity of experimental to loading control (* $p < 0.05$). **(D)** Cells were seeded in 384-well plate and incubated with complete medium (Untreated) or in the presence of 250 μ M H₂O₂ for 2 hours at 37°C. Cells were then pulsed with Alexa-647 Tfn (10 μ g/ml) for 5 min and 10 min, followed by PBS wash, fixed with PFA, and stained with DAPI (nuclear) and CellMask Blue (cytoplasmic). Images were acquired by the Yokogawa confocal microscope. Scale bars, 10 μ m. **(E)** Quantification of cytoplasmic fluorescence intensity per cell, $n = 30$ (** $p < 0.005$).

Figure 7. Localization of Rab5 effectors upon laser-induced mitochondrial damage. BAC GFP-

Rab5 cells seeded on a gridded dish were labeled with MitoTracker-Red CMSRox and photoirradiated as before. Cells were fixed after 30 min post-laser treatment and immunostained with specific ZFYVE20 and EEA1 **(A)**, and APPL1 and APPL2 antibodies **(B)**. **(C)** Quantification of colocalization from untreated and laser-treated cells in **(A)** and **(B)**, $n = 3$. **(D)** Quantification of colocalization between Rab5 and EEA1 as shown in **(A)**, $n = 3$. **(E-F)** BAC GFP-Rab5 cells were treated and processed in the same manner as in **(A)** and immunostained with specific Rabex-5 and Alsin

antibodies, respectively. (G) Quantification of colocalization from untreated and laser-treated cells in (E) and (F), $n = 3$. Scale bars, 10 μm .

Figure 7—figure supplement 1. Localization of endogenous Rabenosyn-5, EEA1, and APPL1/2.

BAC GFP-Rab5 cells were seeded on glass coverslip, fixed, and immunostained with specific antibodies against Rabenosyn-5 (A), EEA1 (B), APPL1 (C), and APPL2 (D). Scale bars, 10 μm .

Figure 7—figure supplement 2. HeLa cells over-expressing GFP-2xFYVE^{Hrs}. Cells were transfected with GFP-2xFYVE^{Hrs} for 24 h, labeled with MitoTracker-Red CMXRos, photoirradiated as before, and then imaged live. Images were capture immediately post-laser (0 min) and after 60 min elapsed time.

Figure 7—figure supplement 3. Localization of Rabex-5 and Alsin in HeLa cells. (A) BAC GFP-Rab5 cells were seeded on glass coverslip, fixed, and immunostained with specific antibodies against Rabex-5. (B) A schematic representation of domain organization of full-length human Alsin. The regulator of chromosome condensation 1 (RCC1), B-cell lymphoma (Dbl) homology (DH) and pleckstrin homology (PH), membrane occupation and recognition nexus (MORN) motif, and vacuolar protein sorting 9 (VPS9) domains are labeled. Three putative GEF domains are annotated. (C) Immunostaining of HeLa cells with specific antibodies against Rab5 and Alsin.

Figure 8. Alsin is required for Rab5 recruitment and regulates cytochrome c release. (A) Flow chart depicting the different stages and time (in days) from iPSC, to neuroprogenitor cells (NPC), and to generating mature spinal motor neurons (sMN). Figure legends indicate the various small molecules and compounds that are used at different stages. (B) WT and Alsin^{-/-} cells were challenged with 100

1108 μM H_2O_2 for 1 hour. Cells were fixed and immunostained with Rab5 and TOM20 antibodies. Inset
1109 images show the representative of the signals from TOM20 and Rab5 under control (left panel) and
1110 H_2O_2 -treated condition (right panel). Scale bars, 10 μm . (C) Subcellular fractionation of cytosolic
1111 (Cyto) and mitochondrial (Mito) fractions from WT and *Alsin*^{-/-} iPSC-sMN treated with either PBS
1112 (control) or 200 μM H_2O_2 for 1 hours at 37°C. Protein samples were loaded onto SDS-PAGE and
1113 immunoblotted with Rab5, tubulin (cytoplasmic loading control), and TOM20 antibodies by Western
1114 blot. (D) Cytosolic fractions were prepared as in Figure 6C from WT and *Alsin*^{-/-} iPSC-sMN
1115 challenged with 200 μM H_2O_2 for 1 hours at 37°C. Densitometric quantification of cytosolic
1116 cytochrome c from Western blot probed cytochrome c antibody. Data were collected from three
1117 independent experiments. Y-axis corresponds to normalized ratio intensity of experimental to loading
1118 control (* p <0.05; ** p <0.005).

1119
1120 **Figure 8—figure supplement 1. Validation of CRISPR/Cas9 *Alsin*^{-/-} cells in induced pluripotent**
1121 **stem cells (iPSC) and iPSC-derived spinal motor neurons (iPSC-sMN).** (A) Electrophoresis result
1122 of the PCR reaction using primers flanking exon 3 and within exon 3. Homozygous deletion was
1123 confirmed by the absence of a 2.8 kb in *Alsin*^{-/-}. (B) Protein lysates from WT KOLF and *Alsin*^{-/-} iPSC
1124 were loaded onto SDS-PAGE and probed with antibody against *Alsin*. A band detected at ~184 kDa,
1125 but absent in *Alsin*^{-/-}, corresponds to full-length *Alsin*. (C) WT KOLF and *Alsin*^{-/-} iPSC and
1126 neuroprogenitor cells (NPC) were immunostained with pluripotency markers Oct4 and Lin28, and
1127 neuroprogenitor markers Sox2 and Pax6, respectively. (D-E) WT KOLF and *Alsin*^{-/-} iPSC-sMN were
1128 immunostained with motor neuron markers such as ChAT, HB9, and ISL1, nuclear dye DAPI, and
1129 cytoskeletal marker MAP2. (F) WT KOLF and *Alsin*^{-/-} iPSC-sMN were immunostained with specific

antibodies against Rab5 and Alsin, along with DAPI (nuclear) and phalloidin (actin) stains. Scale bars, 10 μ m.

Figure 9. Schematic model depicting the role of Rab5-Alsin-mitochondria during oxidative stress. In normal condition, mitochondria (Mito, red) are elongated and tubular (top left). Rab5 (green) are localized on early endosomes (EE) to assemble Rab5 machinery for endosomal maturation and membrane trafficking. At steady state, we observed some EE transiently making contacts with mitochondria. During oxidative stress (eg. laser- or chemically-induced) that leads to MOMP, mitochondria undergo a dramatic morphological transformation into rounded and swollen structures (top right). This is accompanied by an increase in Rab5-positive endosomes forming MCS with mitochondria of less than <5 nm. Release of apoptotic signal such as cytochrome c from mitochondria into the cytosol is associated with Rab5 translocation to the OMM, which is involved in blocking cytochrome c release and caspase activation. The recruitment and activation of Rab5 on mitochondria depend on the Rab5 GEF Alsin (blue), resulting in a selective recruitment of Rabenosyn-5 (light green), in order to regulate apoptosis and confer cytoprotection.

Video 1. Dynamics of transferrin and mitochondria. HeLa cells were labeled with Alexa-488 transferrin (Tf; green) and MitoTracker-Red (Mito; red). Images were acquired using a spinning disk confocal microscope at 11 frames/sec. Time stamp corresponds to min:sec:msec.

Video 2. Dynamics of transferrin and mitochondria. Zoom-in of a HeLa cell labeled with Alexa-488 transferrin (Tf; green) and MitoTracker-Red CMXRos (Mito; red). Movement of endosomes

during a mitochondria fission event is shown. Images were acquired using a spinning disk confocal microscope at 11 frames/sec. Time stamp corresponds to min:sec:msec.

Video 3. Dynamics of Rab5-positive endosomes and mitochondria. Zoom-in of a BAC GFP-Rab5 (green) cell labeled with MitoTracker-Red CMXRos (Mito; red). Images were acquired using a spinning disk confocal microscope at 11 frames/sec. Time stamp corresponds to min:sec:msec.

Video 4. Mitochondria dynamics during laser-induced stress. HeLa cells were labeled with MitoTracker-Red CMXRos and photoirradiated via 561 nm laser for 1 min, and immediately imaged. Time-lapse was acquired using a spinning disk confocal microscope at 11 frames/sec for 5 min.

Video 5. Endosomes and mitochondria interactions upon laser-induced stress. BAC GFP-Rab5 (green) cells were labeled with MitoTracker-Red CMXRos (red) and photoirradiated via 561 nm laser for 1 min, and then imaged after 5 min. Time-lapse was acquired using a spinning disk confocal microscope for 20 frames with 5 sec increment. Boxed regions indicate distinctive GFP-Rab5 endosomes docking onto mitochondria.

Video 6. Mitochondria dynamics during H₂O₂-induced stress. HeLa cells were labeled with MitoTracker-Red CMXRos and then imaged in the presence of 250 μ M H₂O₂ for 60 min. Time-lapse was acquired using a spinning disk confocal microscope for 50 frames with 2 min increment.

Figure 1–Source Data. Numerical data corresponding to the graph presented in Figure 1D.

1175 **Figure 4–Source Data.** Numerical data corresponding to the graph presented in Figure 4G.

1176

1177 **Figure 5–Source Data.** Numerical data corresponding to the graphs presented in Figure 5C,D.

1178

1179 **Figure 6–Source Data.** Numerical data corresponding to the graphs presented in Figure 6C,E.

1180

1181 **Figure 7–Source Data.** Numerical data corresponding to the graphs presented in Figure 7C,D,G.

1182

1183 **Figure 8–Source Data.** Numerical data corresponding to the graph presented in Figure 8D.

1184

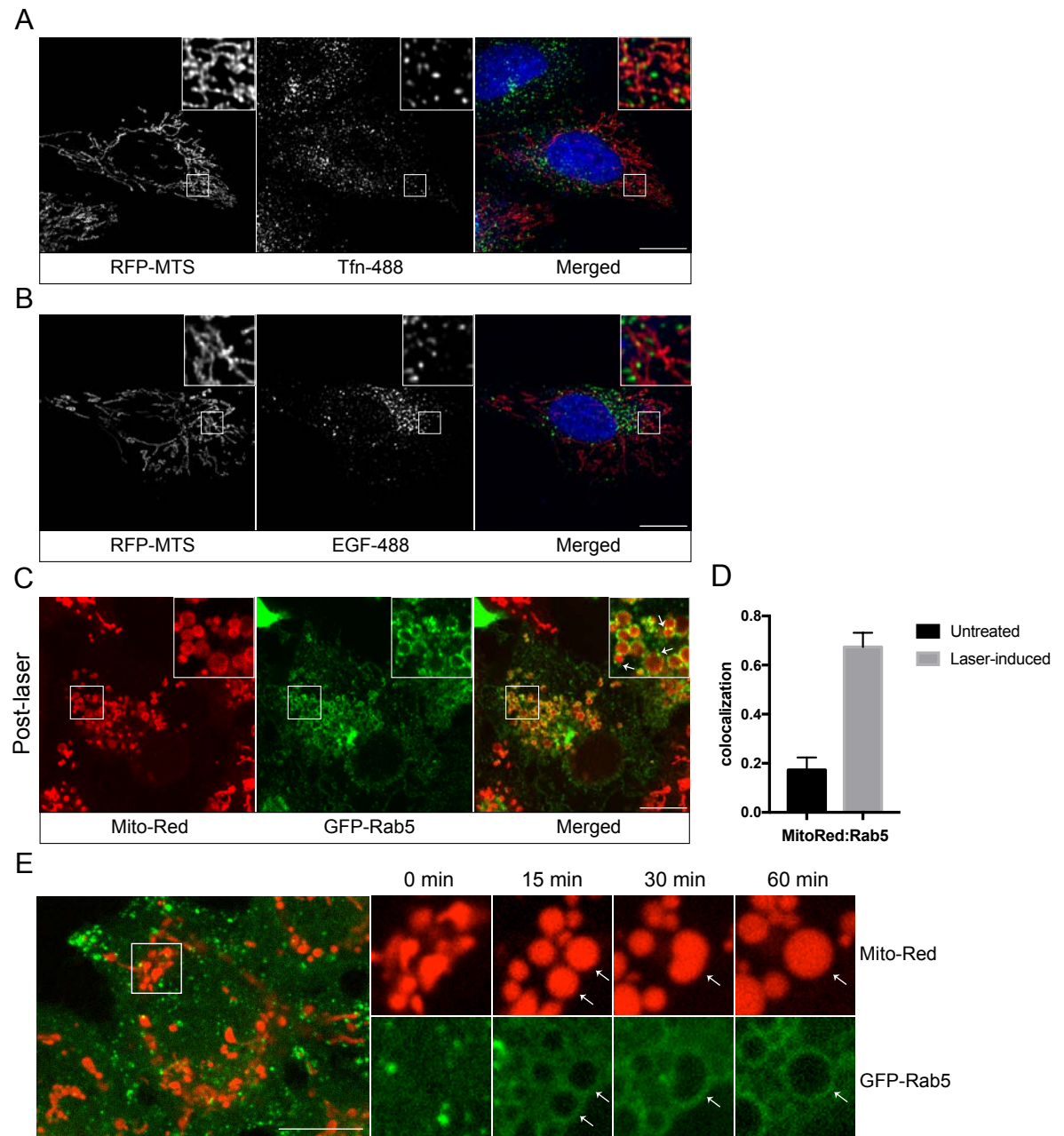


Figure 1

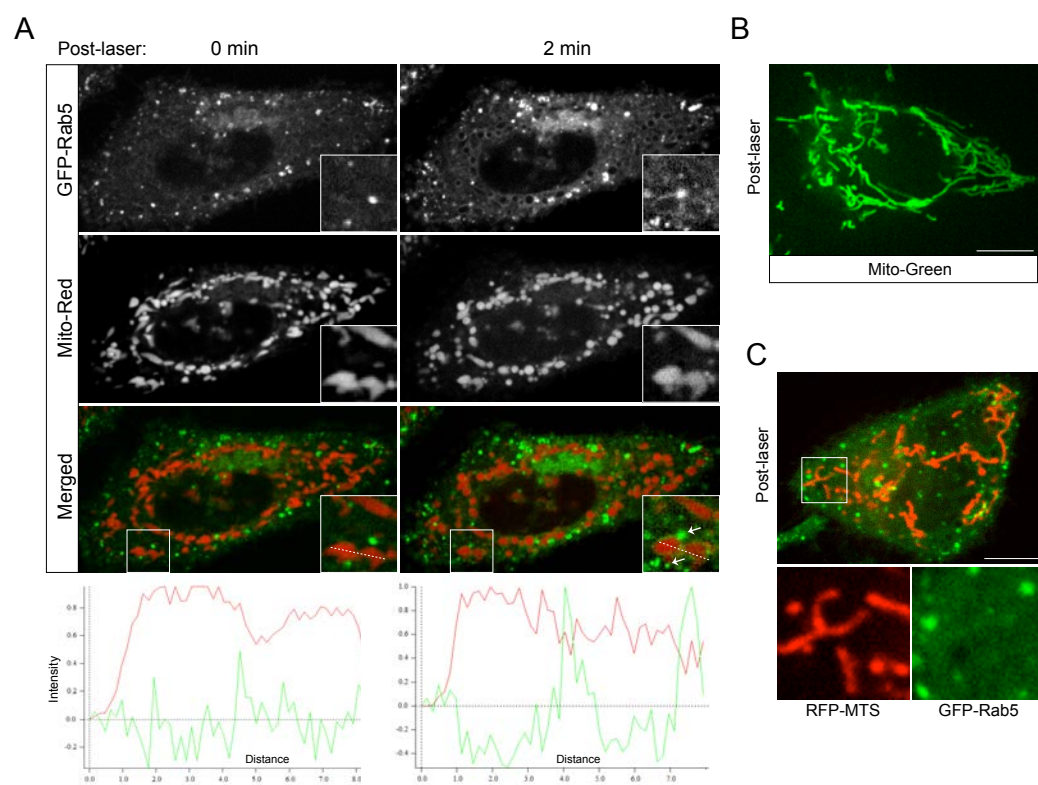


Figure 1–figure supplement 1

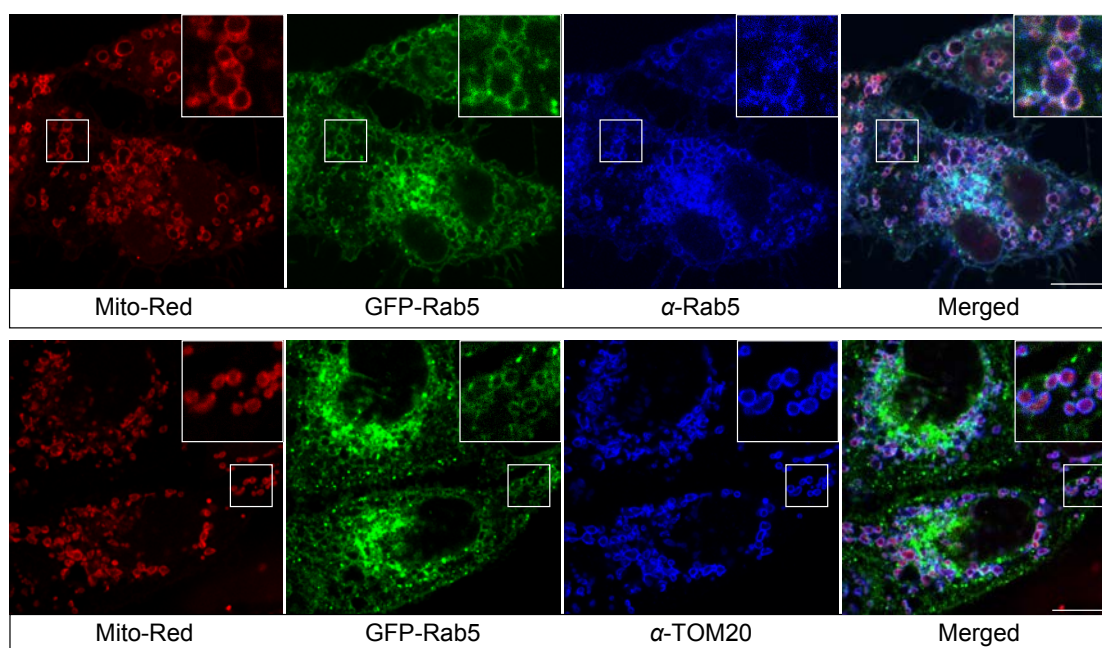


Figure 1—figure supplement 2

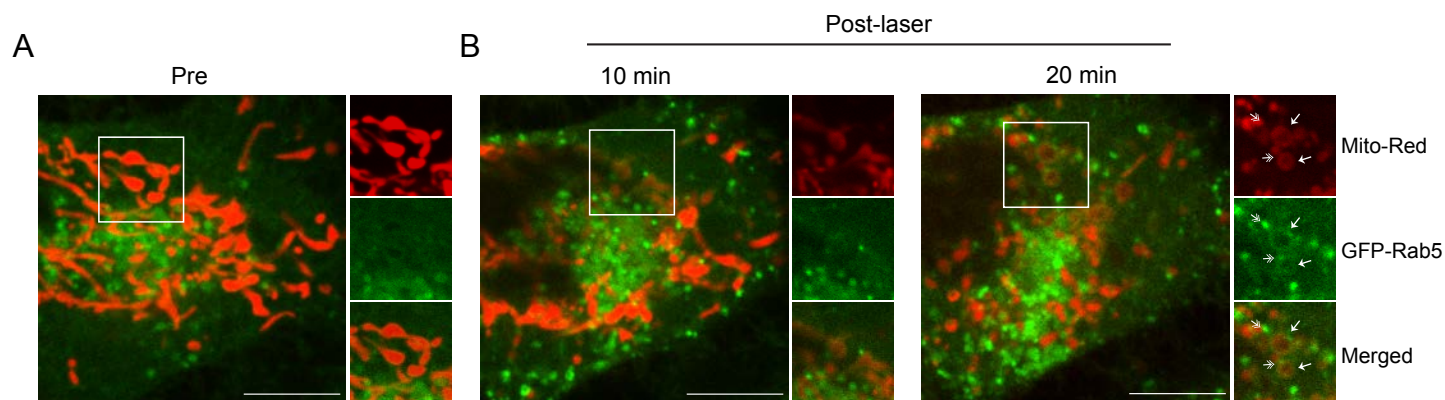


Figure 2

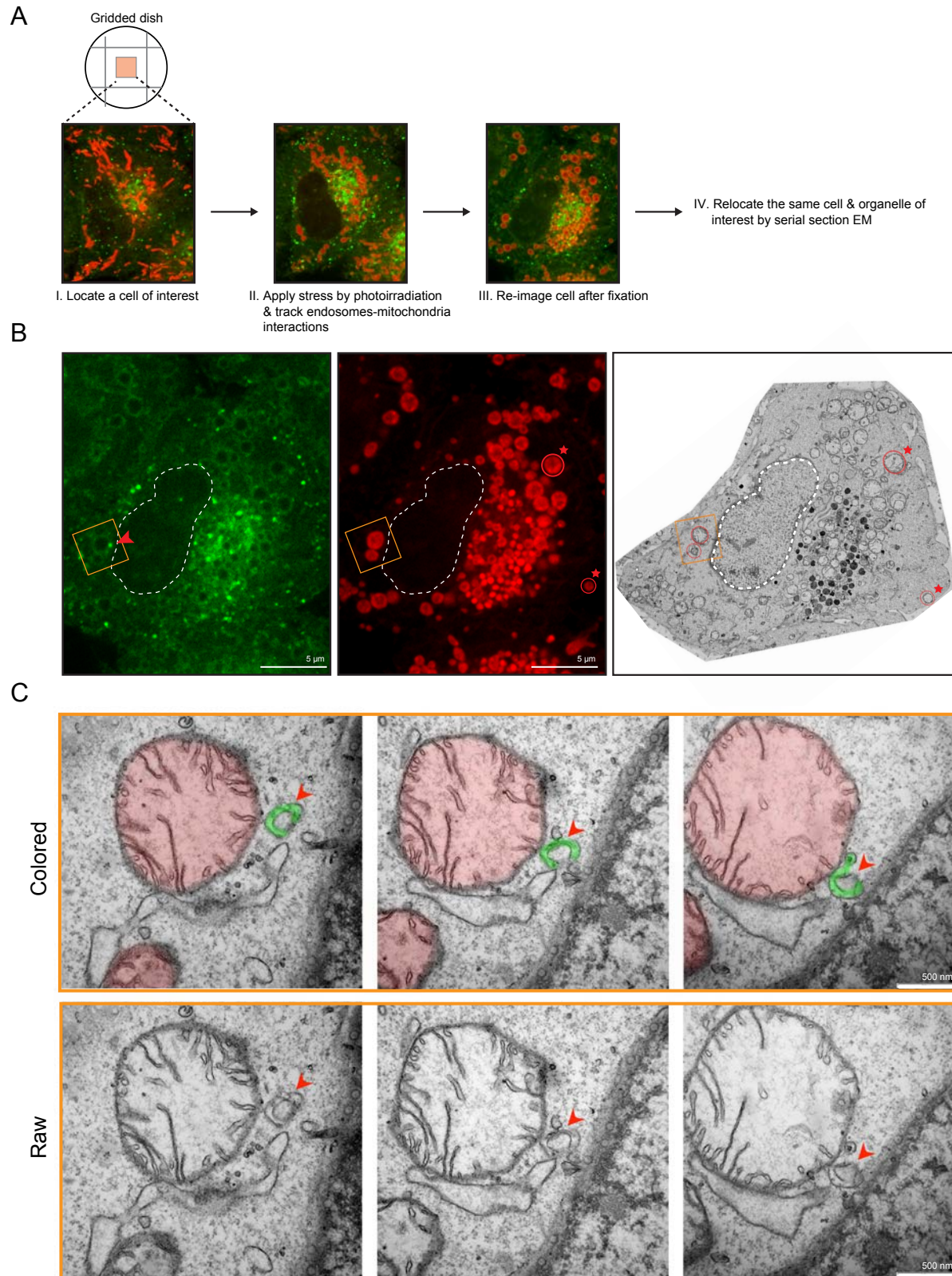


Figure 3

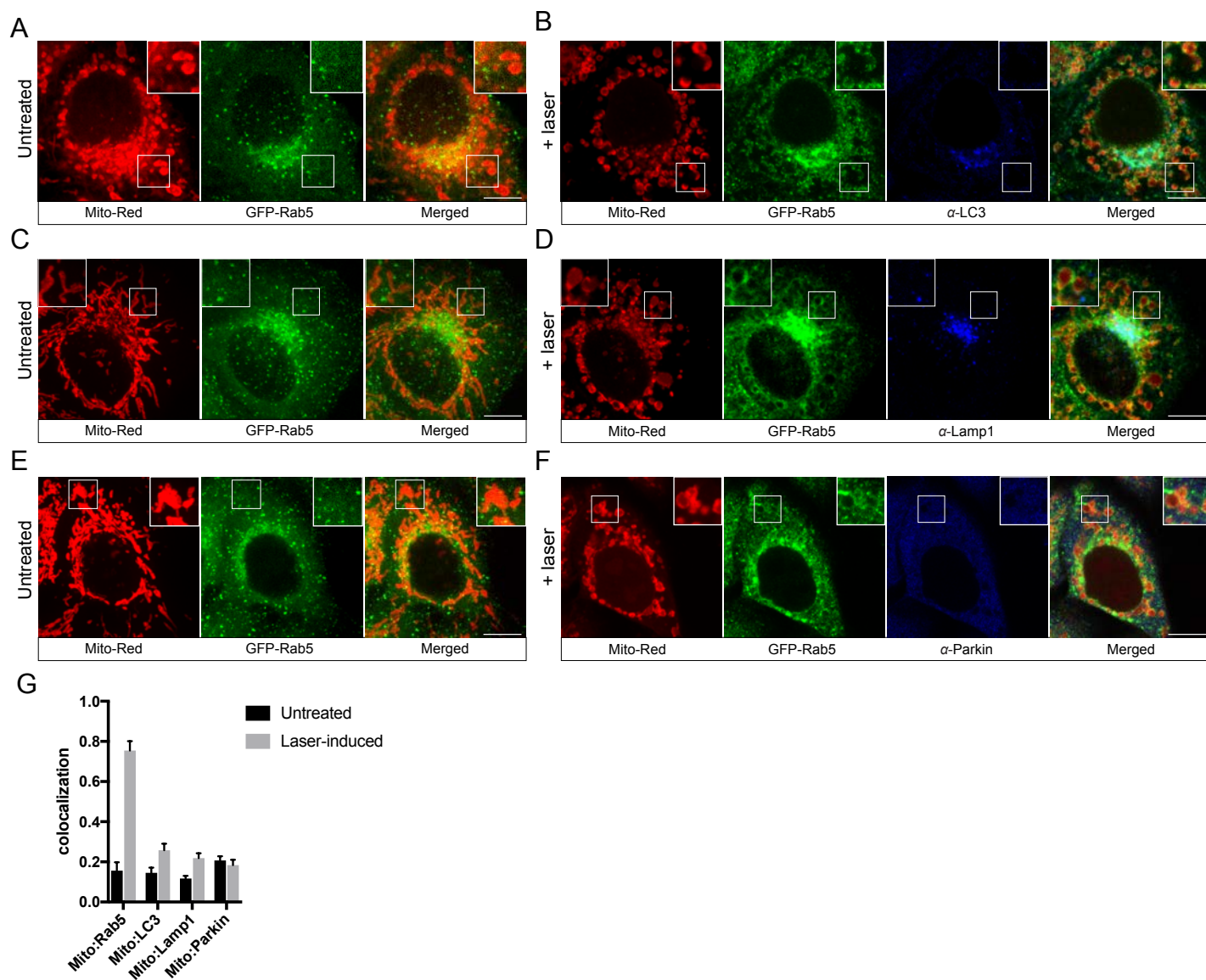


Figure 4

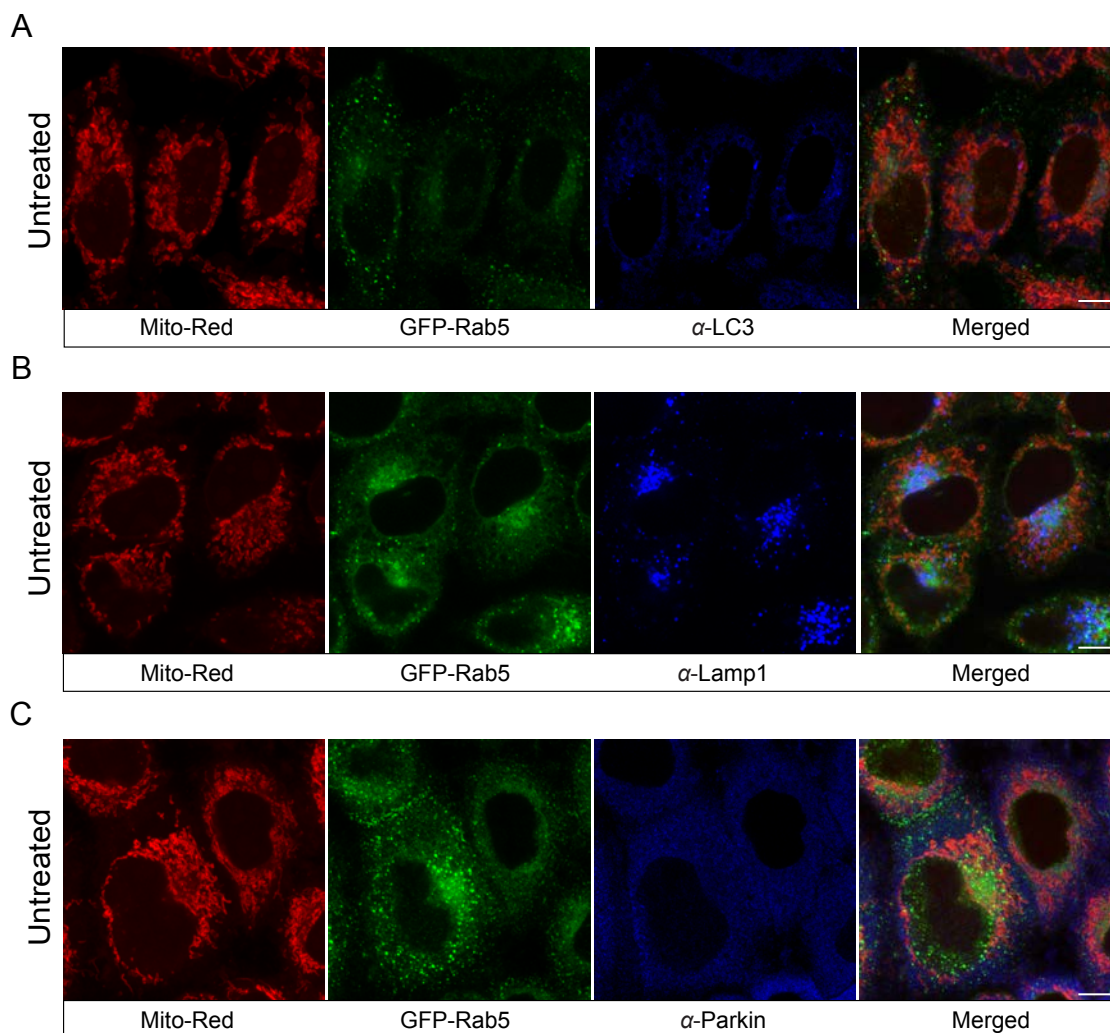


Figure 4—figure supplement 1

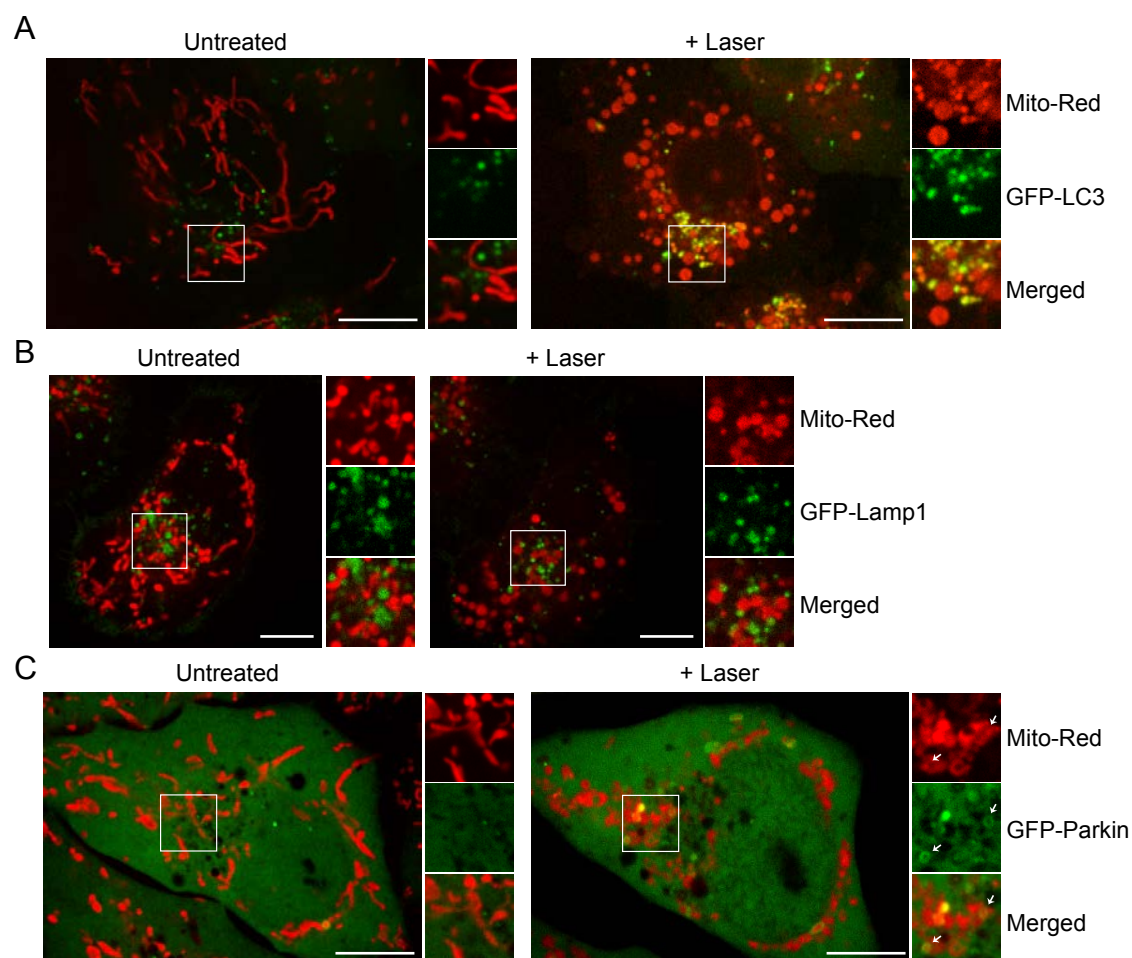


Figure 4—figure supplement 2

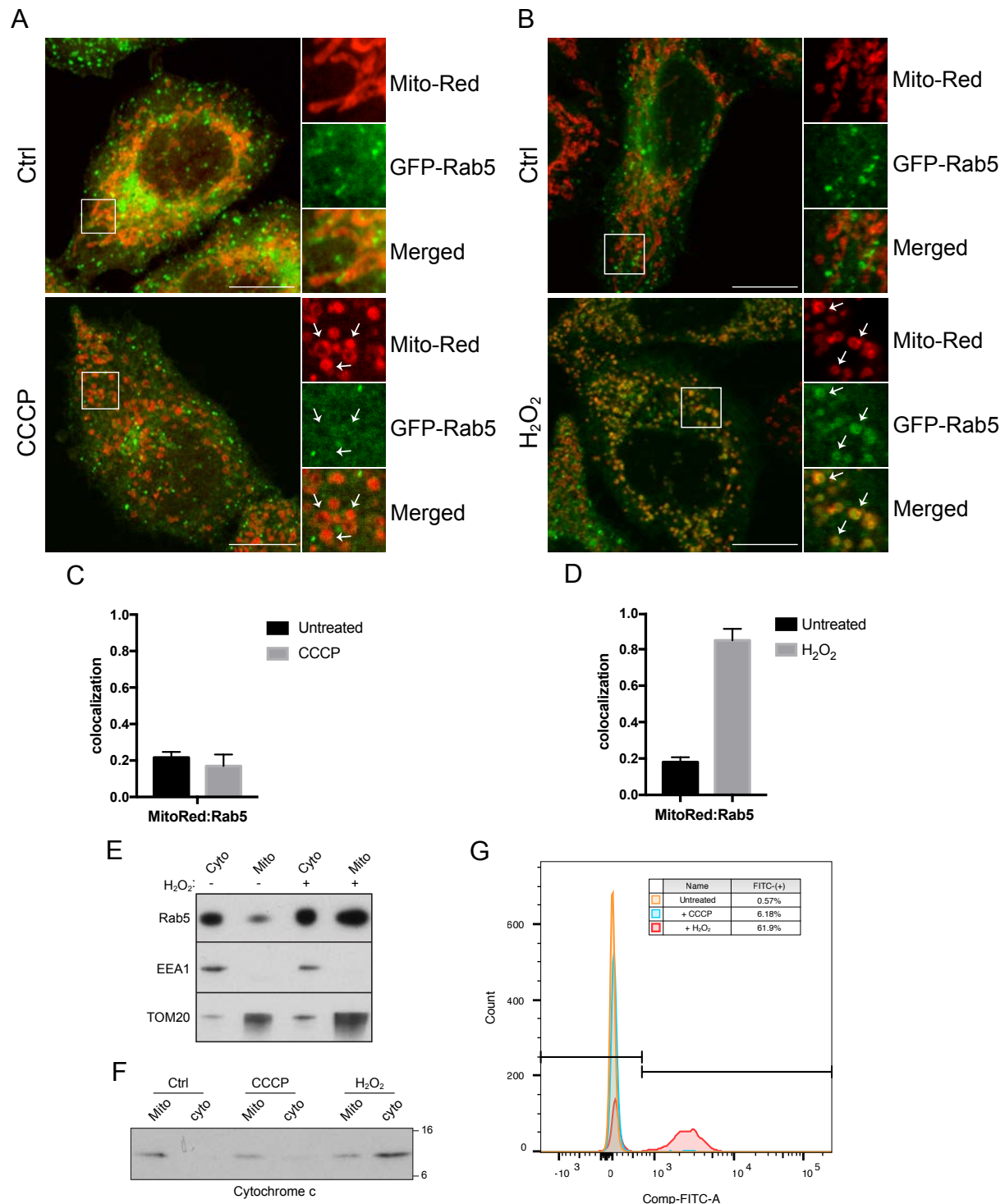


Figure 5

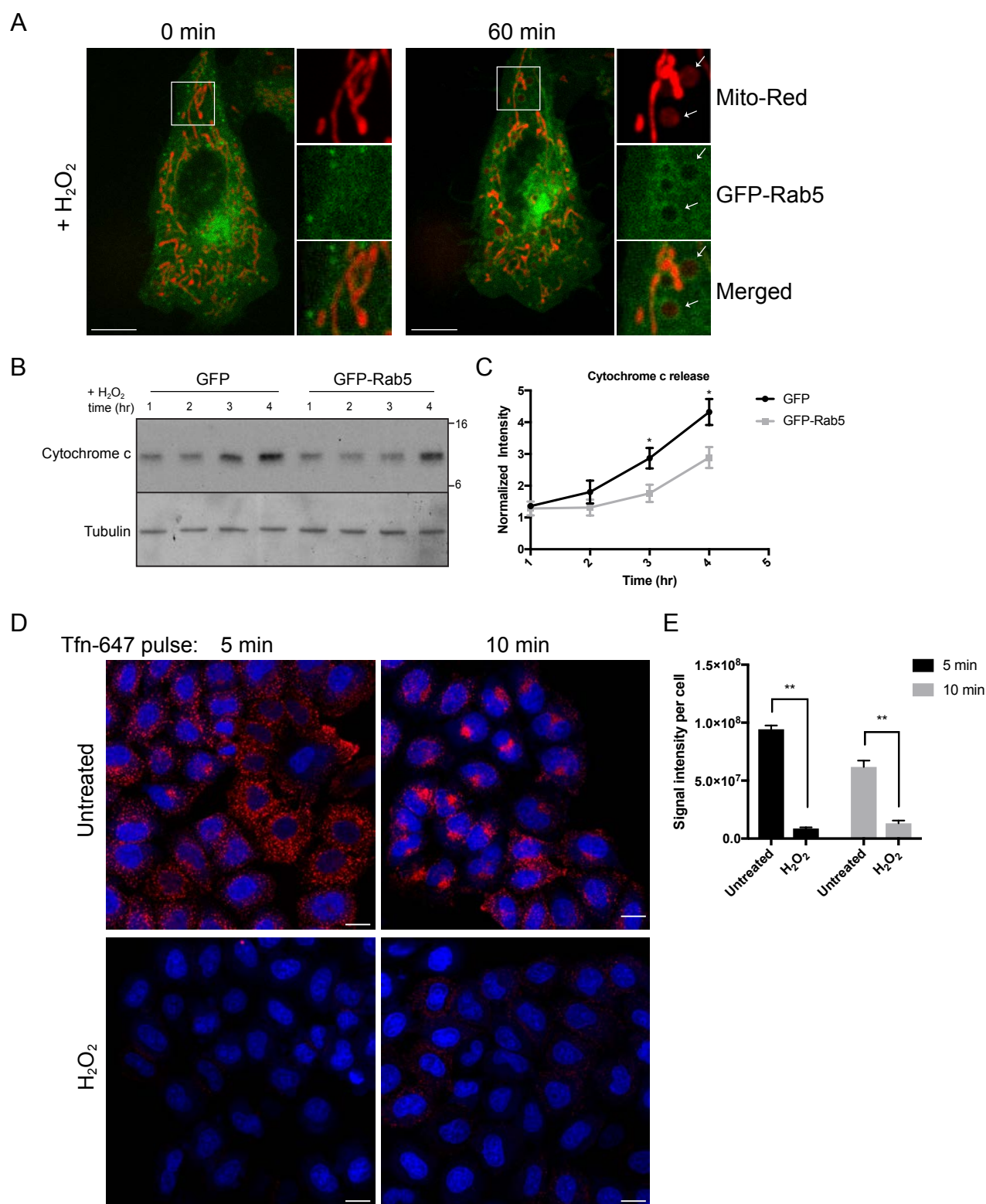


Figure 6

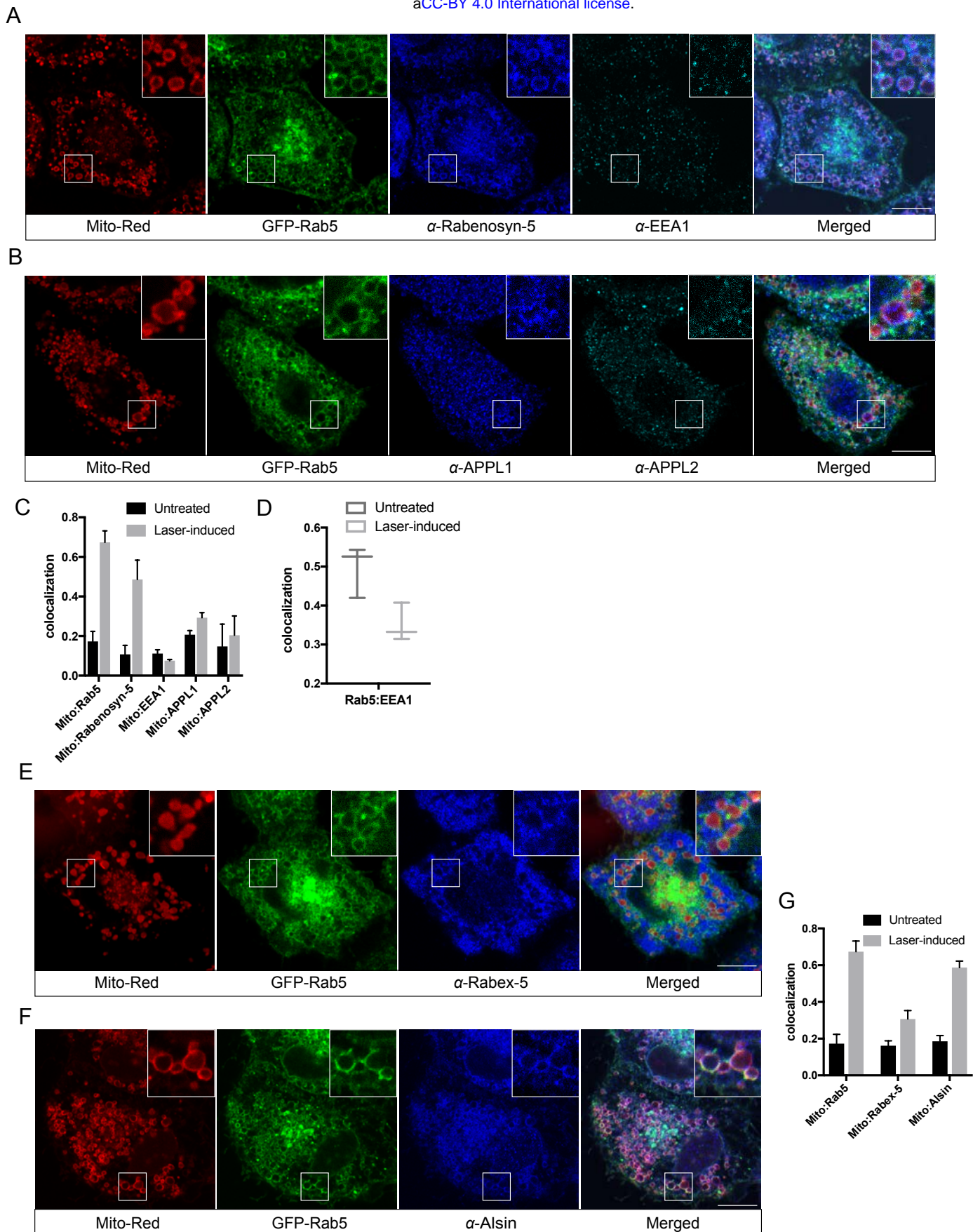


Figure 7

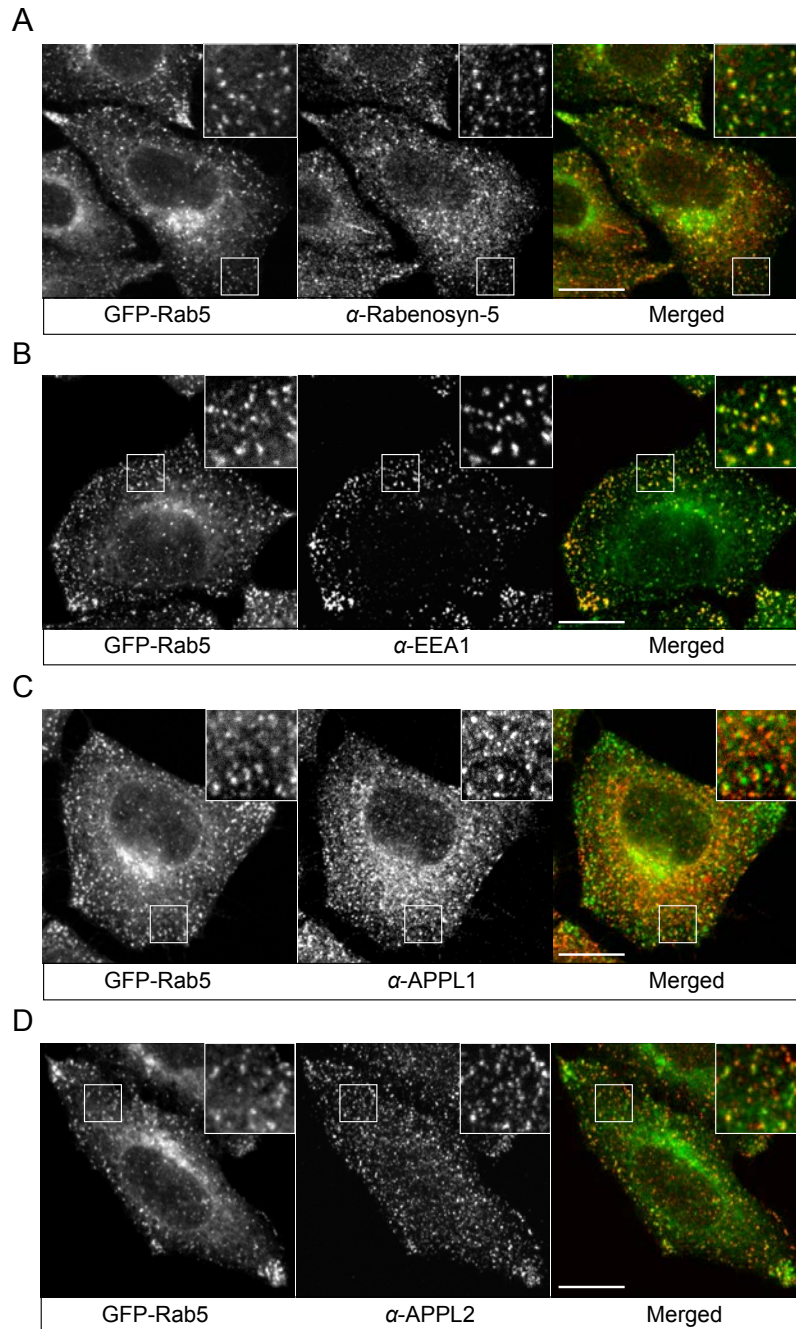


Figure 7–figure supplement 1

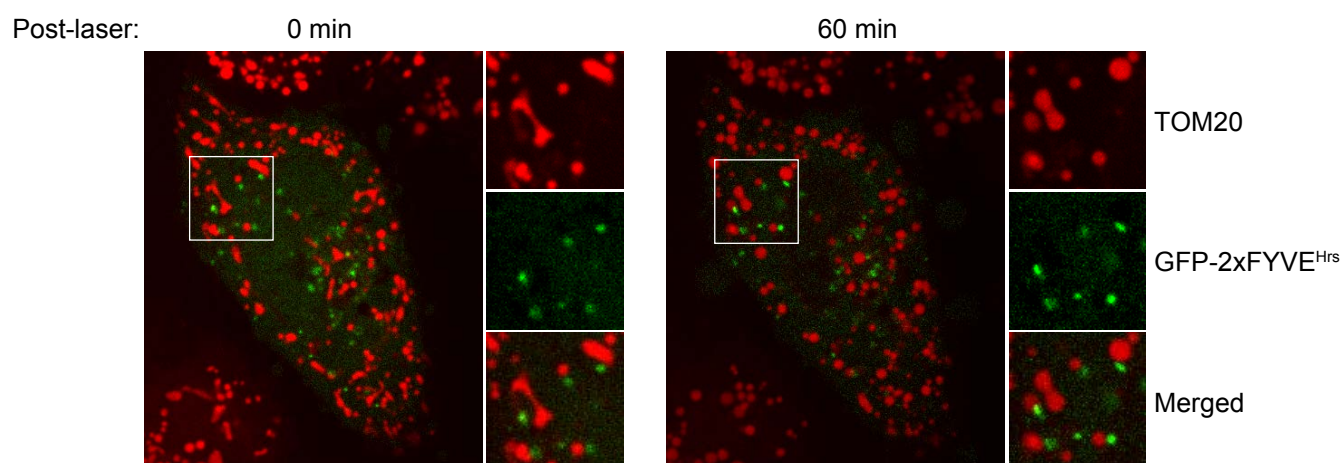


Figure 7—figure supplement 2

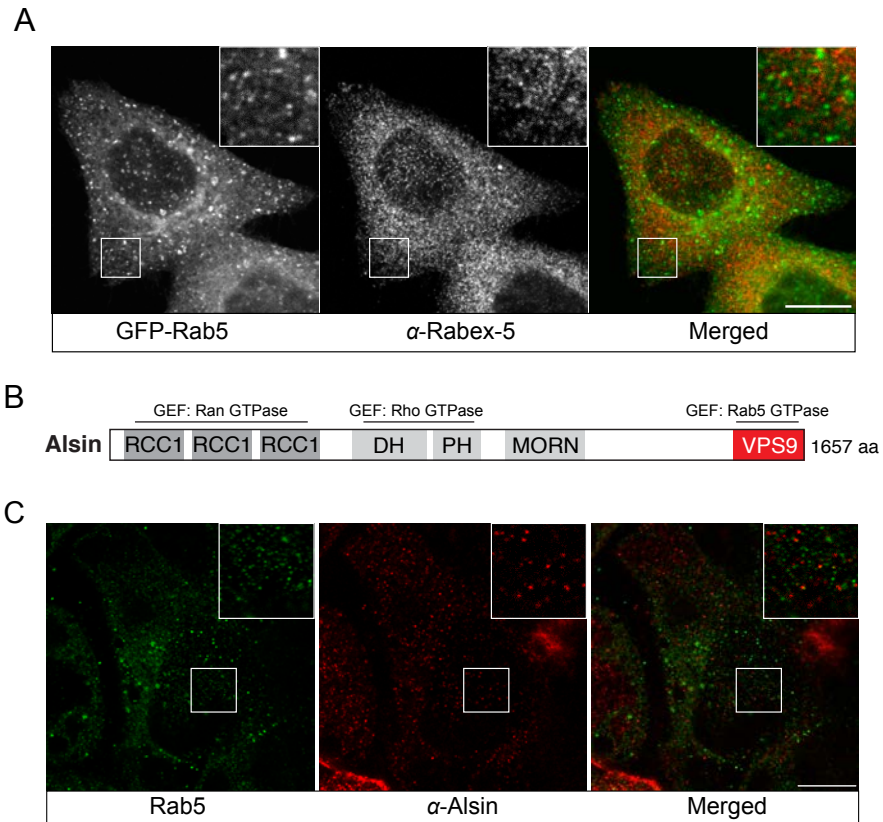


Figure 7–figure supplement 3

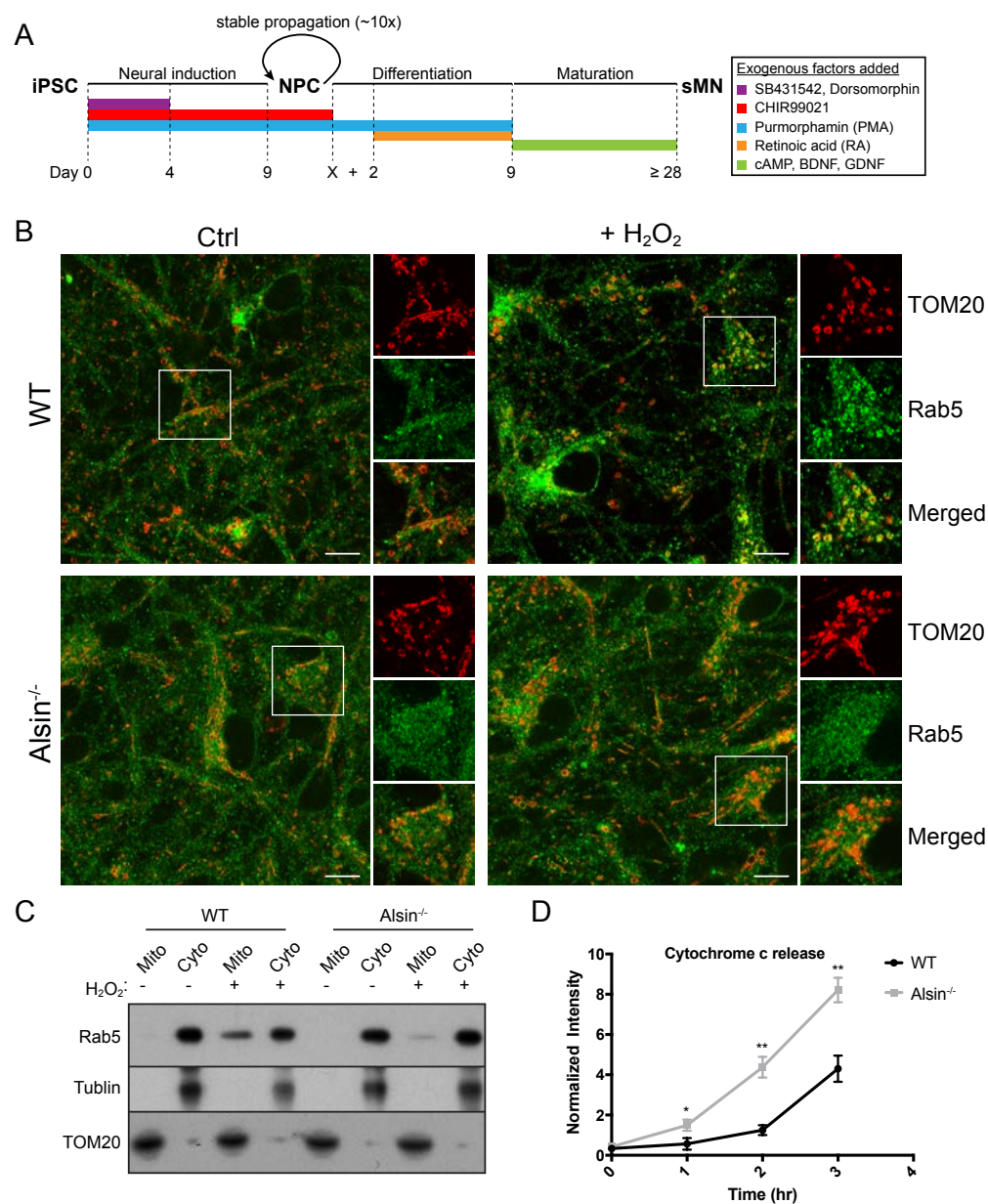


Figure 8

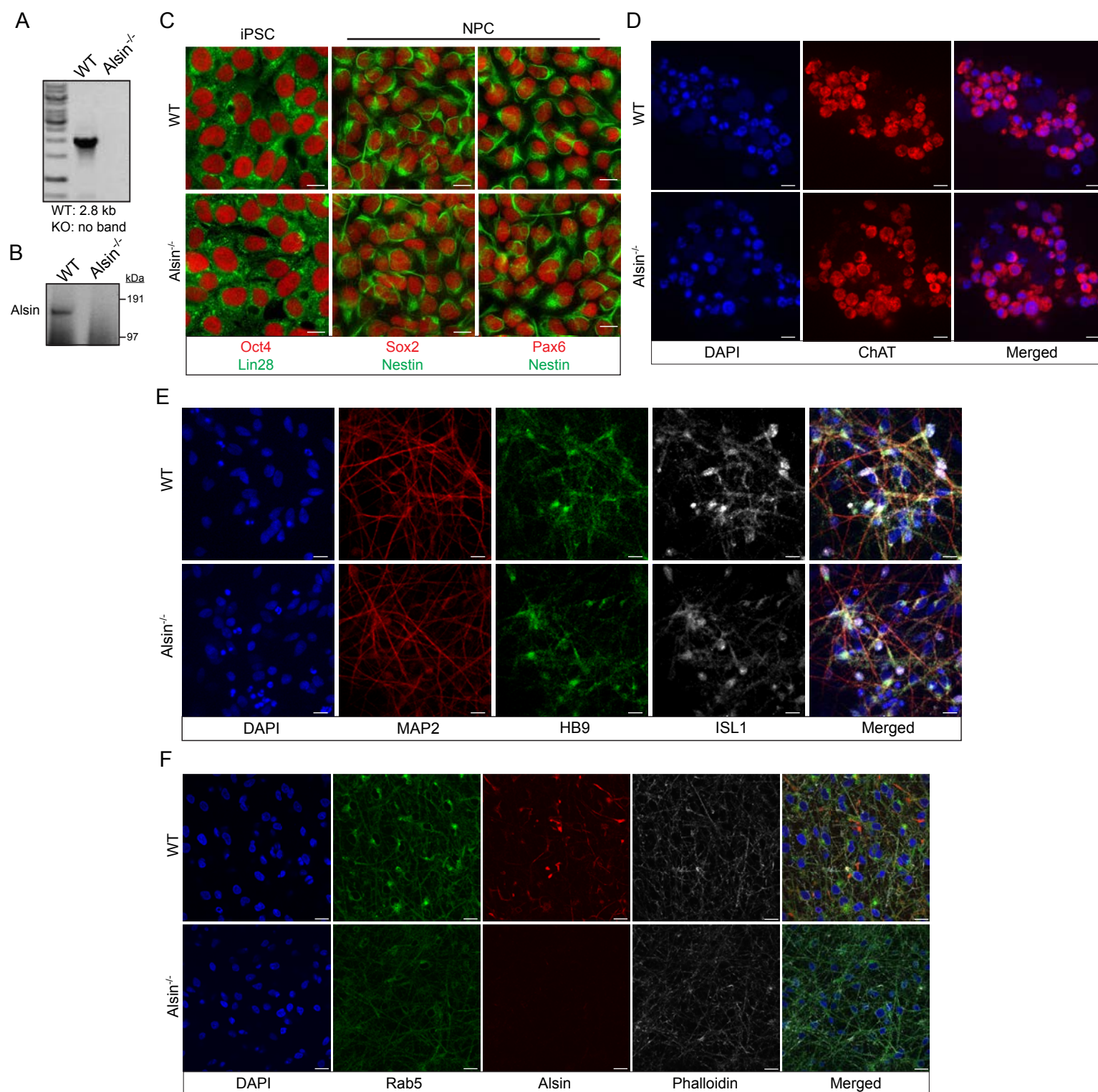


Figure 8—figure supplement 1

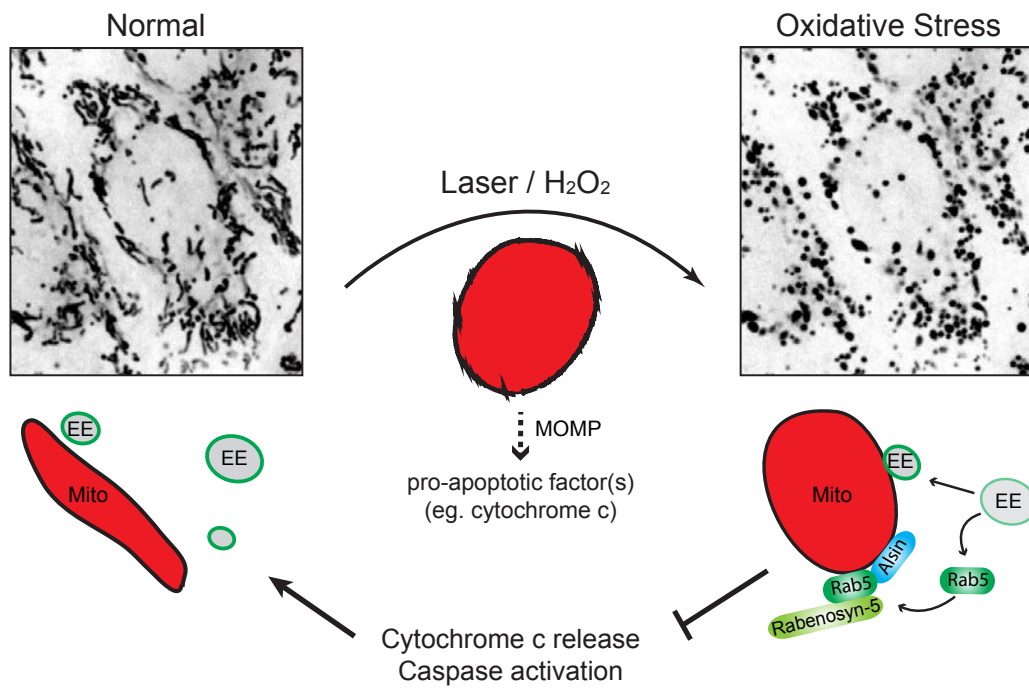


Figure 9